DEVELOPMENT AND APPLICATION OF A MOIRE FRINGE TECHNIQUE TO THE ANALYSIS OF A STRUCTURAL KNEE

b y

C.J. JENKINS, B.E. (Hons.)

submitted in partial fulfilment of the requirements
for the degree of

Master of Engineering Science

UNIVERSITY OF TASMANIA

HOBART.

December, 1965.

ACKNOWLEDGEMENTS

This work was carried out in the Civil Engineering Department of the University of Tasmania. The author wishes to thank all members of staff of the University. In particular the author wishes to thank Professor A.R. Oliver, Professor of Civil Engineering and supervisor of research, E. Middleton and Dr. M.S.Gregory for their helpful advice and encouragement and B.M. Wright who made the master gratings.

SUMMARY

The technique of making inexpensive diffraction gratings of a quality suitable for moire fringe strain analysis is described together with a method of viewing the gratings for best results. The use of a reference grid avoids the need for resolving fine lines. A secondary moire pattern obtained by interfering two primary patterns from different loads is used to measure displacements and eliminates imperfections from the gratings.

The strain and displacement patterns in knee joints tested by this method are described, and some analytical methods of solving for stress and strain distributions are investigated.

I hereby declare that, except as stated herein this thesis contains no material which has been accepted for the award of any other degree or diploma in any University, and that, to the best of my knowledge or belief the thesis contains no copy or paraphrase of material previously published or written by another person, except when due reference is made in the text of the thesis.

CONTENTS

LIST OF FIGURES

NOTATION

x, y, z - cartesian coordinate axes

α - rotation

ε - normal strain (Lagrangian)

ε_x - normal strain in x direction

ε_y - normal strain in y direction

u - displacement in x direction

v - displacement in y direction

γ_{xy} - shear strain associated with x and y directions

σ_x - normal stress in x direction

σ_y - normal stress in y direction

τ_{xy} - shear stress associated with x and y directions

p - pitch of grating

p_m - pitch of model grating before loading

p'_m - pitch of model grating under load

p_r - pitch of reference grating

θ - angle between model and reference gratings before loading

θ' - angle between model and reference gratings under load

θ_x - rotation of a line initially parallel to y axis

θ_y - rotation of a line initially parallel to x axis

W' - moire fringe spacing

ϕ' - inclination of moire fringes to reference grid

f_1, f_2 - functions of x and y, representing grating lines

f_m - function of x and y denoting grating lines on unloaded model

f'_m - function of x and y denoting grating lines on loaded model

f_r - function of x and y denoting reference grating lines

F - function of x and y denoting moire fringes

F_A - function of x and y denoting additive moire fringes

F_m - " " " deformation moire pattern

F_{mr} - " " " initial primary moire

F'_{mr} - " " " primary moire after loading

F_S - " " " secondary moire

k_1, k_2, k_m, k'_m, k_r - constants

K, K_A - constants

β_n - angle between emergent ray of the n^{th} order and a secondary plane.

ξ - angle between incident rays and a secondary plane

n, n_1, n_2 - spectral orders

λ - wavelength of the light

r - resultant spectral order

ρ_p - fractional displacement of grating

B - ratio of brightness of field at point of fractional displacement ρ_p to average brightness of field

B_1, B_2, - brightness components

C_1, C_2 - phase constants

q - order for which gratings are blazed

B - factor depending on amplitude factors of order sequences

a_1 , a_2 - parameters

b_1, b_2 - parameters

E - Young's modulus

G - modulus of rigidity

μ - Poisson's ratio

H - $E(1-\mu^2)$

U - strain energy

C - complementary energy

P - load

V - shear force

M - moment

M_c - moment at inside corner of knee

M_o - moment about line $y = 0$

P - normal force

κ - path of moment (curvature)

t - thickness

ℓ - half-length of beam

d - half-depth of beam

d' - width of knee measured across line of symmetry

m - slope of edges of knee

ϕ - airy stress function

Z_a - section modulus of column

Z_b - section modulus of beam

INTRODUCTION

Knee or mitre joints in rolled steel beams are commonly used in structures, but no exact analytical solution has yet been found. Knees frequently occur in critically stressed regions and while they represent only a small proportion of the material they often absorb a large proportion of the fabrication cost of a frame. The purpose of this study was to develop a method of analysis which, although still approximate, more closely agrees with the behaviour of an actual structure than those at present available. The approach was through experimental models to an approximate mathematical analysis.

All structural analysis is necessarily approximate to some degree. Real structures are far too complex to analyse completely, and hence the design engineer normally begins his analysis by breaking the structure up into various structural elements, basing the breakup on some, often intuitive, idea of the basic structural action of each part of the complete structure. A bridge may be subdivided into parts which act as beams, slabs or columns, depending upon their geometric form and statical action. The analyst must next further simplify the problem by "constructing" a "physical model" of each structural element. For example, the physical model of a beam is normally elastic, and plane cross sections remain plane during deformation. The chief statical action of a beam is to resist bending, and as a first approximation shear deformations are normally stated to be zero. In order to complete the analysis, a mathematical model may be constructed from the physical model, and a numerical solution obtained. This last step frequently involves further simplification and approximation, in particular where exact solution of the resulting equations is impossible or laborious. (1, 2).

We see from the above that for any structure there are three models; the real structure, the physical model and the mathematical model (2). The aim of engineers should always be to continually refine all three in order to produce improved structures. In this refining process there is a large amount of cross-feeding; solution of the mathematical model may suggest improvements to the physical model, which may in turn suggest improvements to the prototype structure. On the other hand, observations of the real structure may well indicate that the physical model does not adequately represent the real structure, and further refinements may be necessary. The greatest problem is,of course, to determine in any particular case just how well the mathematical model does predict the true state of the actual structure. Only when this last piece of information has been determined can a realistic figure for the factor of safety be given.

In many cases the designer has considerable difficulty in deciding how a structural element acts. In other cases the structural action is too complex to be amenable to mathematical solution, and for one or both of these two reasons a scale model may be built. There are, of course, other but less frequent uses of scale models, such as the use of a disc loaded in compression along a diameter as a means of checking the feasibility and accuracy of a new experimental technique, as is described in section 3.3 of this thesis. Another type of model may be called a model of the mathematics; this class of model includes analogues, such as the membrane analogy sometimes used to solve Laplace's equation, as in torsion problems, and also models designed to illustrate a "law". Although these last types of models do have their uses, they have the disadvantage of drawing attention away from the real structure, and focusing attention on the mathematical solution as some sort of "ideal" to which the real structure should correspond.

Of the two common uses for scale models described in the previous paragraph the first use mentioned, that is to obtain ideas about the action of a structure on which to base a mathematical treatment, is normally used only by research workers. The use of scale models to determine a safe working load is more frequent. In this case the mathematics consists of calculating from empirical data, frequently derived from point measurements using strain gauges, and relating the information so derived to the real structure by means of scale factors. The information gained by point measurements can be applied only to the prototype structure, or another geometrically similar one - for example, strain readings at a few points on a beam of rectangular cross-section would not be much help in predicting a safe load of a R.S.J. if the basic statical action of beams was unknown.

Once the rectangular beam problem has been simplified to a physical model which describes the beam as being elastic with plane cross-sections remaining plane during deformation, the position has been reached where the more complex problem of the R.S.J. may be attacked. It is a well known fact that simple beam theory leads to satisfactory estimates of the behaviour of beams of most cross-sectional forms subject to certain conditions of loading, span/length ratio, etc.

The so-called engineering theory of bending referred to above is an example of a problem which has been attacked with success from the geometric side- the geometry of the deformed structure is first defined, and the results of this definition compared with the external statics of the system to obtain an approximation for the stresses and strains. Another case where the shape has been used in this way is in calculation of the Euler buckling load for a slender pin-ended column. On the other hand a more usual approach to stress analysis has been to describe the stress distribution by some

means or another (e.g. by an Airy stress function) and hence solve from the boundary conditions.

With the possible exception of photoelasticity, all methods of experimental stress analysis are in reality methods of experimental strain analysis. Most of these techniques give only point by point strain readings over a finite gauge length, and hence give no direct indication of the overall deformations of the structure, nor do they afford adequate means of observing stress concentrations. Photoelasticity and moire methods share the advantage of being large-field methods, but the moire method alone has the advantage of giving directly the deformed shape of the model. For this reason the moire methods of experimentation are probably the most powerful yet devised for basic structural research. Furthermore they have the advantage that experimental results are very simply reduced to stress and strain patterns, whereas reduction of photoelastic results requires somewhat tedious numerical computations. (in this context the phrase "moire methods" is intended to include related methods of measuring geometry, such as the photogrid method (3) and the Salet-Ikdea technique for measuring slope contours (4).)

This thesis describes how the author developed a method whereby moire displacement patterns are used to construct mathematical models of knee joint behaviour. The functional form of the moire curves for a particular knee joint was observed, and used to make guesses of the geometric behaviour of the knee joint under load. These guesses, being based on the overall pattern of behaviour, and containing several free parameters, should give solutions for a wide range of knee shapes and sizes with a similar order of precision to that with which they describe the knee joint on which they were based.

The sensitivity of the moire method of measuring displacements is limited primarily by the grid spacing - a shift of one fringe in the moire pattern produced by grids of 1000 lines/inch corresponds to a displacement of 0.001 inches in the direction normal to the grid lines. Grids used by workers in this field have been largely of the slit-and-bar type, which consist of opaque lines and transparent interline spaces. These gratings have been produced by photographic means, the finest in current use being of 1000 lines/inch, what appears to be the useful limit for photographically produced gratings. Unfortunately most common model materials start to yield or creep at strains from 0.001-3 in/in, and hence grids of 1000 lines/in and more are desirable in order to obtain a useful number of fringes over the field of view without using refined experimental techniques.

Guild (5, 6) has described the metrological uses of moire fringes produced by transmission type diffraction gratings produced by the Merton-N.P.L. process. (7, 8, 9). Gratings of this type are, however, expensive (although rather cheaper than those produced by conventional ruling engines) and are not of a suitable form for attaching to model surfaces. A large part of the work described in this thesis consisted of developing a simplified method by which gratings of 1000 and 3000 lines/inch were quickly and cheaply produced in the form of thin perspex films suitable for glueing directly onto models, giving a sensitive moire method with only the simplest of experimental techniques and equipment.

1. THE USE OF MOIRE FRINGES IN STRAIN ANALYSIS

1.1 Introduction

Although the first scientific observation of moire fringes was recorded by Lord Rayleigh in 1874 (10), the widespread use of the phenomenon has only occurred during the past decade. Rayleigh was interested in the possibility of using the fringes as a test of diffraction grating quality, and such a test has been described by Guild (5). Some idea of the many engineering uses of moire fringes may be gauged from references (6, 11-36), while the scientific uses of moire fringes are also growing, particularly in crystallographic studies with the electron microscope. Theocaris (37) has written a bibliography of the more important material published in the field of moire fringe techniques up to 1962.

Moire fringes are produced by "interference" between sets of regularly spaced lines of similar spacing and orientation, such as are shown in fig. 1. The effect is the same as that produced by watered silk, from which the technique takes its name. Moire patterns may also be produced by lines or grooves which are invisible to the naked eye - the moire fringes described by Rayleigh were produced by slit-and-bar type diffraction gratings of 3,000 and 6,000 lines/inch.

For moire fringe strain analysis one grid is attached to the model surface, and a second grid is normally held parallel to, and in close proximity with this model grating. The moire pattern produced, or the changes in the pattern, may then be used to interpret the deformations of the surface during loading. In the case of transparent models, transmitted light may be used for illumination, but for opaque models reflected light must be used. Unless otherwise stated, all remarks contained in this work apply to transmission type setups, although the statements made are not necessarily restricted to this class of problem.

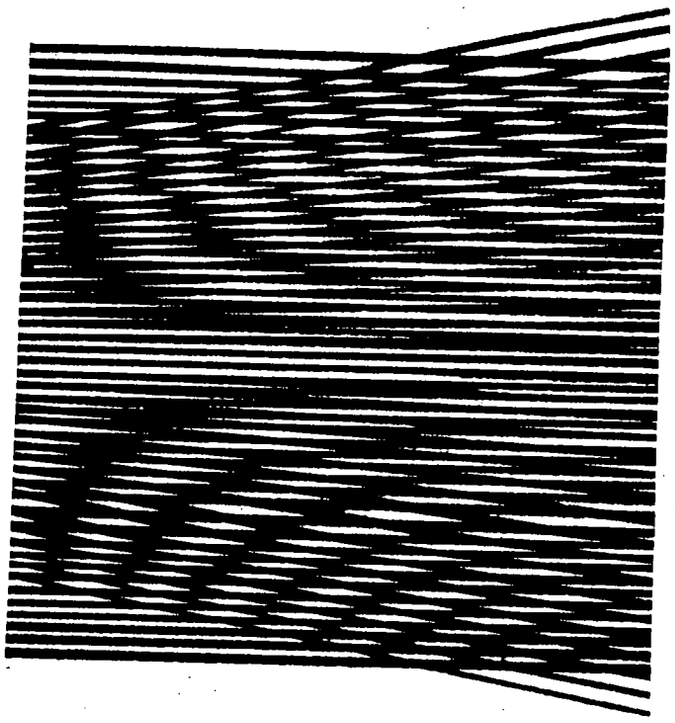

FIG.I MOIRÉ FRINGES.

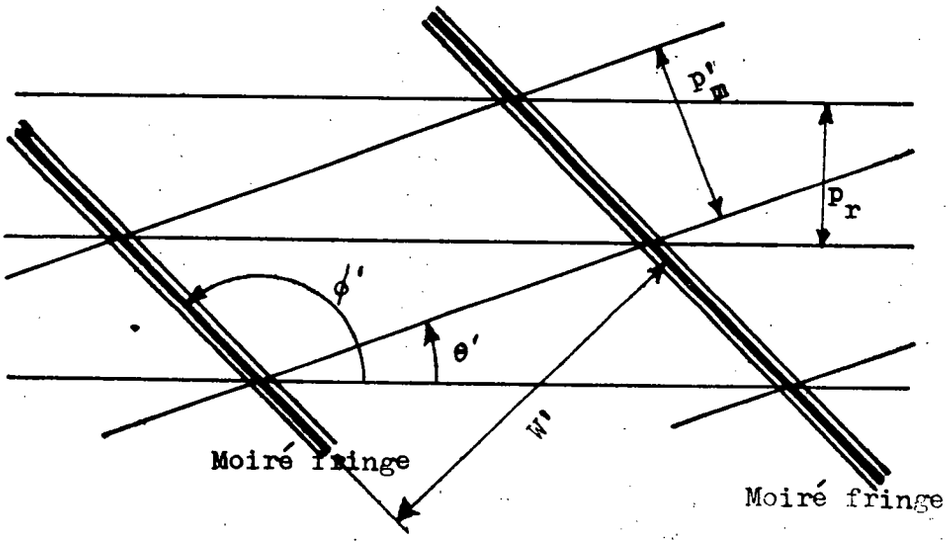

FIG.II MOIRÉ FRINGE GEOMETRY.

1.2 Geometric Interpretation of Moire Fringe Patterns

1.2.1 General

There are two different approaches to moire fringe strain analysis. These have been called the "geometric" method and the "displacement field" method (38). The former method was apparently also the first historically. It was first used by Rayleigh (10), and has been used by Tollenard (39), Guild (5, 6) and Weller and Shepherd (40) for the interpretation of displacement measurements. Kaczer and Kroupa (41) were the first to use the method for strain measurements.

The "displacement field" method of attack was first used by Dantu (14), but was restricted to small deformations. Subsequent work by Dantu (42) and by Sciammarella (38) and Durelli has generalised the interpretation.

Although these methods of analysis are fully treated elsewhere, a brief summary will be included here for the sake of completeness. This summary will be continued to small deformations. It should also be emphasised that the discussion in this section is strictly speaking limited to non-diffracting line networks. However, as will be pointed out later (section 1.3) diffraction gratings produce fundamental fringes which behave exactly as those from non-diffracting grids, but there is the possibility that multiple fringes will be produced.

1.2.2 The Geometric Method of Interpretation

The geometric approach to moire fringe strain analysis is fully treated by Morse, Durelli and Sciammarella (43).

Briefly, the method consists in relating the moire fringe slopes and spacing with the pitch and orientation of the reference grid in order to determine strains. The results apply only to a homogeneous strain field, but can obviously be used for small elements of a non-homogeneous strain field provided deformations are small.

Under the simple conditions outlined in section 1.1 above, it is normal for the reference and model grids to be arranged so that initially

$$p_m = p_r$$

and $$\theta = 0$$

where p_m = model pitch

p_r = reference pitch

θ = initial angle between grid lines.

Now if the fringe spacing after loading is W', the inclination of the fringes to the reference grid is ϕ' and the model pitch after loading is p_m',

then (see fig. 2)

$$\left.\begin{aligned} W' &= \frac{p_m' \sin\phi'}{\sin\theta'} \\ \tan\phi' &= \frac{p_r \sin\theta'}{p_r \cos\theta' - p_m'} \\ p_m' &= \frac{p_r \sin(\phi' - \theta')}{\sin\phi'} \end{aligned}\right\} \quad \text{(i)}$$

where θ' = final angle between grid lines.

ϕ', W' and p_r can all be measured, and the above relations used to find p_m' and θ' at a point. The normal strain in the direction perpendicular to the reference grid rulings is given by

$$\varepsilon = \frac{p_m' - p_r}{p_r} \qquad \text{(ii)}$$

where ε denotes the conventional (or Lagrangian) strain.

In order to analyse the complete strain pattern, two sets of moire patterns are generally (44) required with the grids orientated in different directions. These directions are normally chosen so that the grid lines are first located parallel to the y axis in the x, y plane, and then parallel to the x axis. The strain and rotation in the first case will be

$$\varepsilon_x = \frac{p_m' - p_r}{p_r}$$

$$\theta_x = \theta'$$

and in the second case

$$\varepsilon_y = \frac{p_m' - p_r}{p_r}$$

$$\theta_y = \theta'$$

where ε_x = normal strain in x direction.

ε_y = normal strain in y direction.

θ_x = rotation of a line initially parallel to y axis.

θ_y = rotation of a line initially parallel to x axis.

(θ_x and θ_y should both be measured using the same sign convention e.g. counterclockwise rotations positive).

The rigid body rotation α will be given by

$$\alpha = \tfrac{1}{2}(\theta_x + \theta_y) \qquad \text{(iii)}$$

and the shear strain, γ_{xy} by

$$\gamma_{xy} = \theta_x - \theta_y \qquad \text{(iv)}$$

or by

$$\gamma_{xy} = \tfrac{1}{2}(\theta_x - \theta_y) \qquad \text{(iva)}$$

depending upon the definition of shear strain adopted. The former definition will be used throughout this thesis as being the one adopted by Timoshenko (45).

1.2.3. The Displacement Field Method of Interpretation

The displacement field method of attack is closely related to the "parametric" theory of moire fringes (46, 47). A review of the parametric theory will therefore be given first.

Consider two families of lines in the x, y plane defined by the functions

$$f_1(x, y) = k_1$$

and

$$f_2(x, y) = k_2 \qquad \text{(v)}$$

where k_1, k_2 vary according to some rule, e.g. k_1 , k_2 take integral values. Two such families are sketched in fig. 3, together with the moire which would be formed by these curves. It is apparent that the equation representing the moire pattern is given by

$$F(x, y) = f_1(x, y) - f_2(x, y) = k_1 - k_2 = K \qquad \text{(vi)}$$

We note from fig.3a that the moire has been drawn along the shorter of the two diagonals of the areas formed by the original families f_1 and f_2. We could have drawn the moire along the longer of the two diagonals, and obtained the equation to the moire

$$F(x, y) = f_1(x, y) + f_2(x, y) = k_1 + k_2 = K_a \qquad \text{(via)}$$

This moire is known as the additive moire, the former being known as the subtractive moire. In all present moire techniques the additive moire has no physical significance. The moire which is actually seen is always the one with the widest fringe spacing, and for the small rotations such as are present in normal strain analysis, this moire is fortunately always the subtractive moire. A full description of moire fringes in general, including additive moires has been given by Pirard (46).

The treatment given above shows the simplicity (and the power) of moire fringe techniques. With the exception pointed out in the previous paragraph, moire fringes always show the difference between two sets of lines. Thus when a reference grid and a deformed model grid produce moire fringes, these fringes represent equal increments of displacement in the direction perpendicular to the reference grid lines.

The truth of this statement is best illustrated by reference to fig.3b. The two grids shown were initially identical and superimposed so as to produce no fringes. During deformation point A has remained fixed. Point B, and all points on the fringe passing through B have obviously been displaced one grid pitch in

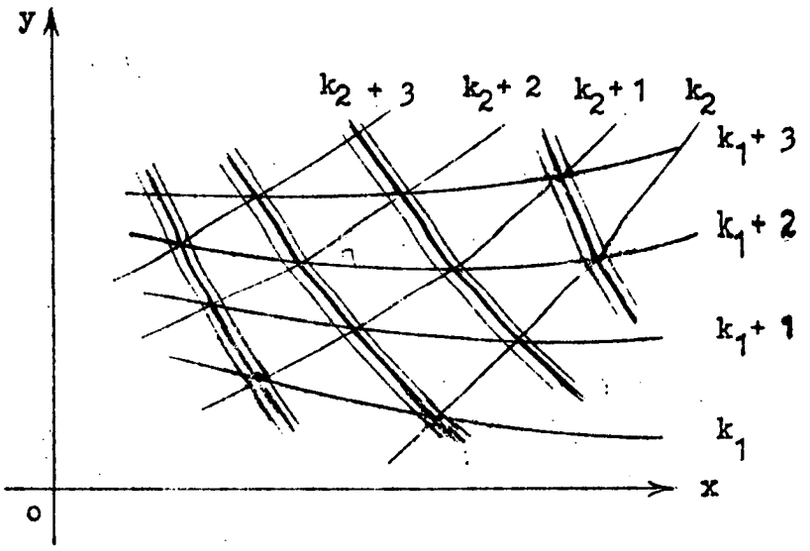

a. Moire fringes from two line networks.

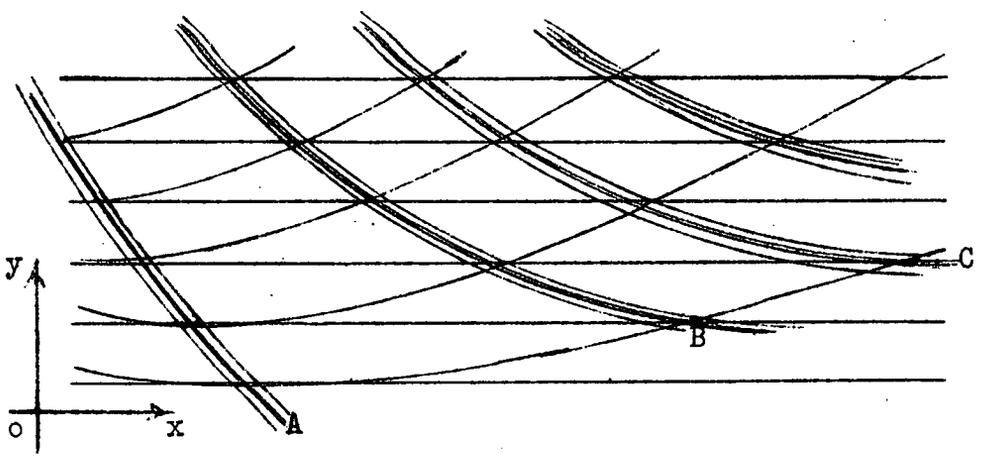

b. Moire fringes as lines of constant displacement.

Fig. 3. The Displacement Field Interpretation of Moire Fringes.

the direction perpendicular to the reference grid lines. Similarly all points on the fringe passing through C have moved two grid pitches. Since the grid lines have been drawn parallel to the x axis, the fringes represent increments of displacement in the y direction, which we shall represent by the symbol v. Similarly we shall use u to represent displacements in the y direction.

With two moire patterns, one of u and one of v, strains can be calculated (usually by graphical differentiation) using the relationships (45)

$$\left.\begin{aligned} \varepsilon_x &= \frac{\partial u}{\partial x} \\ \varepsilon_y &= \frac{\partial v}{\partial y} \\ \gamma_{xy} &= \frac{\partial v}{\partial x} + \frac{\partial u}{\partial y} \end{aligned}\right\} \quad \text{(vii)}$$

and the rigid body rotation is given by

$$\alpha = \tfrac{1}{2}\left(\frac{\partial v}{\partial x} - \frac{\partial u}{\partial y}\right)$$

Strictly speaking these relationships give the Eulerian description of strain, but for small deformations the Lagrangian and Eulerian descriptions are essentially the same.

The above description of Dantu's displacement field method is necessarily brief. More complete arguments, and the extension of the theory to include large deformations are contained in Dantu's papers (14 -18, 42) and also in a paper by Sciammarella (38). There are, however, two further points which should be mentioned here. Firstly, it is not essential that the two sets of grids used to produce the moire patterns be orthogonal, but the accuracy and simplicity of the method are both shown to best advantage by this system. Secondly, since displacement is a vector quantity, displacements in any direction may be found by vector addition. By this means strains in any direction can be found without recourse to the Mohr's circle construction or similar means which are necessary when dealing with a tensor quantity. The interpretation of moire patterns in general, including a discussion of singularities and symmetry relationships has been presented by Durelli, Sciammarella and Parks (44).

1.3 Moire Fringes produced by Diffraction Gratings

1.3.1 Differences between Slit and Bar and Ruled Diffraction Gratings

Grids normally used in moire fringe work are of the slit-and-bar type, produced by photographic means. This type of grid acts on the incident wavefront to give amplitude variations in the various parts of the emergent wavefront.

The gratings used in the writer's work have been of the normal spectroscopic type. These have grooves ruled in the surface, and hence the transparency is essentially the same all over the ruled surface. The action of this type of grating depends on phase variations in the emergent wavefront, amplitude variations, if any, being purely incidental. In slit-and-bar type gratings it is the phase variations which are accidental.

The following description of the action of spectroscopic gratings is only an outline. The subject has been fully covered in two books by Guild (5, 6) from which most of the information in the next sections has been derived.

1.3.2 A single Diffraction Grating

It is necessary first to define two planes associated with any plane diffraction grating.

A principal plane is a plane perpendicular to the rulings.

A secondary plane is a plane perpendicular to both the grating plane and the principal planes.

Consider now collimated light incident on a single grating. The relationship between the directions of the incident rays and emergent rays of the n^{th} order is

$$\sin\beta_n - \sin\xi = \frac{n\lambda}{p} \qquad \text{(vii)}$$

where β_n = the angle between the emergent n^{th} order rays and a secondary plane,

ξ = the angle between the incident rays and any secondary plane

n = the spectral order

p = the grating pitch

λ = the wavelength of the light.

From equation vii it is apparent that the number of emergent orders may be large - the total number is either *

---

*$[\,]$ means "the integral part of ".

$$\left.\begin{array}{l} \left[\frac{2p}{\lambda}\right] \\ \text{or} \quad \left[2p/\lambda\right] + 1 \end{array}\right\} \qquad \text{(viii)}$$

depending upon the angles of emergence.

1.3.3 A Pair of Gratings in Series

When two identical gratings are separated by a small uniform air gap and have their rulings parallel, each of the emergent beams from the first grating vecomes an incident beam on the second. It will readily be seen from equation (viii) that if the first grating splits the light into N separate orders, then the second grating will split each of these orders into N or N + 1 orders. Denoting the order numbers from the first grating by n_1 and those from the second by n_2, then each of the orders, r, in the resultant spectrum will be composed of all the orders n_1 and n_2 such that

$$n_1 + n_2 = r \qquad \text{(ix)}$$

e.g. the order number 3 produced by the grating pair will be made up of orders

(0, + 3), (+1, +2), (+2, +1), (+3, 0), (+4, -1) etc.

Under the conditions we have specified the resultant spectrum is identical to that which would be produced by a single grating. Here we are more interested in the case where there is a small pitch difference between the two gratings, and where there is a small angle between the rulings of the grating.

Before proceeding, further definitions are required.

A principal median plane is one which bisects the angle between two principal planes, one from each grating.

A secondary median plane is one which is perpendicular to both the grating surfaces and the principal median planes.

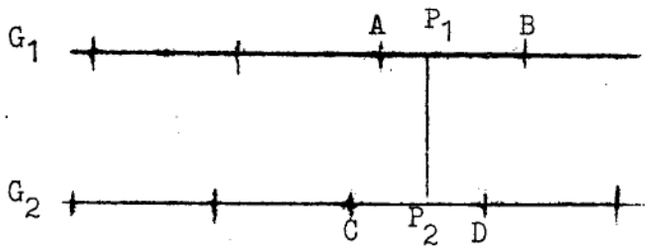

Fig. 4. Two Gratings in Series

Fig. 4 shows a normal section through two gratings, G_1 and G_2; the bars on G_1 and G_2 represent the initial points of the rulings at the section. The fractional positions of two points, P_1 and P_2 in the rulings are AP_1/AB and CP_2/CD and are independent of the angle at which the section is taken. The <u>fractional displacement</u> ρ_P of G_2 with respect to G_1 at the point P_2 is defined by

$$\rho_P = \frac{AP_1}{AB} - \frac{CP_2}{CD} \qquad (x)$$

(Note that ρ_P can take values only in the range -1 to +1).

When two gratings are illuminated by collimated monochromatic light at an arbitrary angle of incidence, the ratio, B_ρ, of the brightness of the field at points of fractional displacement ρ_P to the average brightness of the field is given by

$$B_\rho = 1 + \sum_{1}^{n-1} B_n \cos(C_n - 2n\pi\rho) \qquad (xi)$$

where $B_1, \ldots B_{n-1}$ = brightness components whose magnitudes are determined by the amplitudes and phases of the order sequences involved in the emergent beam.

n = number of emergent order sequences emerging from second grating

$C_1, \ldots C_{n-1}$ = phase constants depending upon the differences in path lengths of the inverted order sequences as they pass through the air gap.

When used to measure displacement and strains these gratings are arranged to be mirror images of each other, and are viewed under the condition known as minimum deviation. When the angles that the incident beam and the emergent beam of the order under consideration make with a secondary median plane are equal and opposite the deviation of the beam is a minimum, and hence this condition is known as the condition of minimum deviation (5, 6). Under this condition the phase constants, C_n , in equation (xi) are zero, and the expression reduces to

$$B_\rho = 1 + \sum_1^n B_n \cos 2\pi n\rho \qquad \text{(xii)}$$

From this equation it can be seen that the characteristics of the resulting moire fringe system depends upon the relative magnitudes of the coefficients B_1 , ... , B_{n-1}. These magnitudes are determined by the groove shape of the gratings. With course gratings the number of emergent orders is large (about 90 for gratings of 1000 lines/inch; see equation viii). Under these conditions there is a strong possibility of multiple fringes and multiple beam fringe sharpening in some of the orders owing to the higher harmonic terms in the intensity function, equation xii.

Generally speaking, the multiple fringes are of no particular benefit, since their distribution, both as regards intensity and spatial distribution is normally irregular. However the fringe sharpening effect can be of great benefit, since the centre of the fringes may be found by eye with greater accuracy than is possible with fringes having a sinusoidal variation of intensity. Unfortunately, with the multiple beam systems the average intensity of the field is low, and photographic reproduction becomes difficult.

In order to increase the average intensity of the transmitted light, gratings may be "blazed" so that the light is concentrated into a few orders. To achieve this the groove is given a sawtooth form, the angle of the sawtooth depending upon the wavelength of the

incident light. If the gratings are heavily blazed for one order the intensity function reduces to

$$B_\rho = 1 + B \cos 2(2q-r)\pi\rho \qquad \text{(xiii)}$$

where r = resultant order

q = order for which gratings are blazed

B = factor depending on the amplitude factors of the order sequences q, r-q and r-q, q.

Since the q^{th} order dominates, fringes of fundamental period can be seen where $r = 2q + 1$ or $4 = 2q - 1$. Where $r = 2q$ no fringes will be seen since the period is now infinite. By blazing in two adjacent orders (which are normally low orders for practical reasons) the intensity function can be reduced to

$$B_\rho = 1 + B\cos 2\pi\rho \qquad \text{(xiv)}$$

If the gratings are blazed for the two orders q and $q+1$, the bright, fundamental fringes will be seen in the resultant order $2q + 1$.

In practice the groove form and other factors cannot be controlled sufficiently to make the intensities of all but one or two orders negligible, as the above argument may have implied. However gratings can be designed and made in which the one or two orders dominate sufficiently to cause behaviour which approximates to that outlined above.

1.4 Experimental Techniques and Apparatus used in Moire Fringe Strain Analysis

1.4.1 The Simple Moire Fringe Technique

As has been mentioned previously, most moire techniques for strain measurement use coarse grids, with perhaps 300-1000 lines/inch. These grids are of the amplitude type, and are printed on to the model by photographic techniques.

The simplest moire fringe strain analysis technique is carried out using identical grids for model and reference. The reference grid is placed as close to the model as practicable and initially the lines on both model and master are parallel. After deformation the moire fringes are photographed and analysed by either of the methods described in section 1.2. Only the simplest of apparatus is required, both for illumination and photography when the grids are of 3-600 lines/inch. Transparent or opaque models may be used. Provided the optical system and film have sufficient resolving power to photograph the individual grid lines the reference grid may be dispensed with, and the model grid used as its own reference by exposing the film twice, once while the model is unloaded, and once while it is loaded.

At 1000 lines/inch writers report difficulty in photographing the fringes. Under the simple conditions of illuminating and photographing the fringes diffraction effects are troublesome, and hence monochromatic light is used, and a vacuum is necessary to ensure intimate contact between the reference and model grids after loading (27). In addition, photographic reproduction of grids as fine as 1000 lines/inch is troublesome, and involves the use of expensive equipment (48). For these reasons almost all moire fringe analysis has been carried out using grids of less than 1000 lines/inch; most work in fact appears to have been carried out using grids in the 3-600 line/inch range. The result has been that the technique has been largely limited to elastic studies with low-modulus materials such as urethane rubber, (43) and to studies in the plastic region.

In the next section some of the methods aimed at increasing the sensitivity and accuracy of the moire fringe technique will be described.

1.4.2 Some Refinements to the Simple Moire Technique

Two methods have been used to increase the accuracy of the moire method. The first of these aims at increasing the number of fringes in the field by using grids of different pitch for model and reference grids. The apparent initial strain or mismatch must be subtracted from the final apparent strain to determine the true strain, but the existence of a large number of fringes in the field allows greater accuracy in the plotting of the displacement curves (and hence in the graphical differentiation to obtain the strain) than would be possible with the simple moire technique. This method has been used by several authors (28,32,49), and has recently been described by Chiang (48), who also extended the method to include initial mismatch caused by giving the reference grid a rotation with respect to the model grid.

The other method of increasing the accuracy of the moire fringe technique is related to the comparator technique used in photoelasticity (50, 51) and involves the determination of fractional fringe values. Guild (6) has described electronic instruments designed to split fringes produced by spectroscopic (or phase-type) diffraction gratings in a homogeneous strain field. More recently Sciammarella (52, 53) has described a method of splitting fringes produced by slit-and-bar (or amplitude) type gratings in a non-homogeneous strain field. The method allows a considerable increase in the accuracy obtainable with course grids, and is, moreover, capable of extension to fine grids of the spectroscopic type. Unfortunately both these methods require specialised equipment, and high quality gratings.

2. PRODUCTION OF THE GRATINGS

2.1 Introduction

The method used to produce the gratings was a modification of the Merton-N.P.L. process for manufacturing diffraction gratings (7-9, 54-57). Gratings suitable for the type of work described in this paper need not be of spectroscopic quality, and this allowed considerable simplification of the original process.

The process used may be briefly summarised as follows. A helical groove of the desired pitch was first cut on a brass cylinder, and then the periodic errors in the pitch of this groove were eliminiated using a Merton Nut (which is essentially a specially designed chasing nut) to produce a master grating on the brass. By pouring a solution of perspex over the cylinder, and stripping the resultant grating replica, gratings were obtained in the form of a thin film.

2.2 The Master Grating

2.2.1 Preliminary

The master gratings were made in a 17" swing lathe . This lathe was chosen because its size and rigidity presumably reduced vibration and also because rack feeds as low as 0.001"/rev were available without modification of the change gears. Alterations to the change gear ratio gave feeds down to 0.00011"/rev allowing gratings as fine as 9000 lines/in to be contemplated.

The gratings were cut on 2" diameter brass bar, the length varying between 10 and 12 inches. These bars were given no special heat treatment or surface finishing, but were merely trued and given a finishing cut with a diamond tool. Once this truing cut was made, it was found essential that the work remained in the lathe to preserve the centering. For this reason all surface examination was carried out with the aid of a stereoscopic microscope mounted on the toolpost of the lathe by means of a bracket. The power of

this microscope (up to 160X) was found adequate for preliminary checks of surface quality and groove form.

The initial thread used to drive the Merton Nut was of similar saw-tooth form to that of the final groove, but was rather deeper. For the 1000 line/inch gratings made during the preliminary work high speed tool steel and tungsten carbide were both tried for the tool material. The groove cut with these materials was sufficient to drive the Merton Nut, but the tools were incapable of retaining their original sharpness and form for the full length of cut. Better results have been obtained since by using diamond tools.

This initial thread was cut at a lathe speed of 47 r.p.m. since this was the slowest available. No work has as yet been carried out to determine the optimum speed for this or any of the other cuts made during the preparation of the master grating.

2.2.2 The Merton Nut

The grooves cut as described above possessed all the periodic and progressive errors from the lathe rack feed. The Merton Nut acted as a chasing nut, and by averaging over many threads produced a groove almost free from periodic errors in pitch.

The Merton Nut used consisted of a split tube which clamped three timber blocks to the cylinder by the end grain faces. These blocks were $2\frac{1}{2}$" long x $\frac{5}{8}$" wide by $\frac{5}{8}$" thick and were made from Huon Pine, an indigenous Tasmanian fine-grained softwood. The ends of the blocks were lubricated with a thin film of P.T.F.E. tape. A stiff arm with a ball race on the end rested on the tool post and prevented the nut from turning. The cutting tool was mounted firmly on the end of the nut. Figs. 5, 6, 8 show the Merton Nut in its final form.

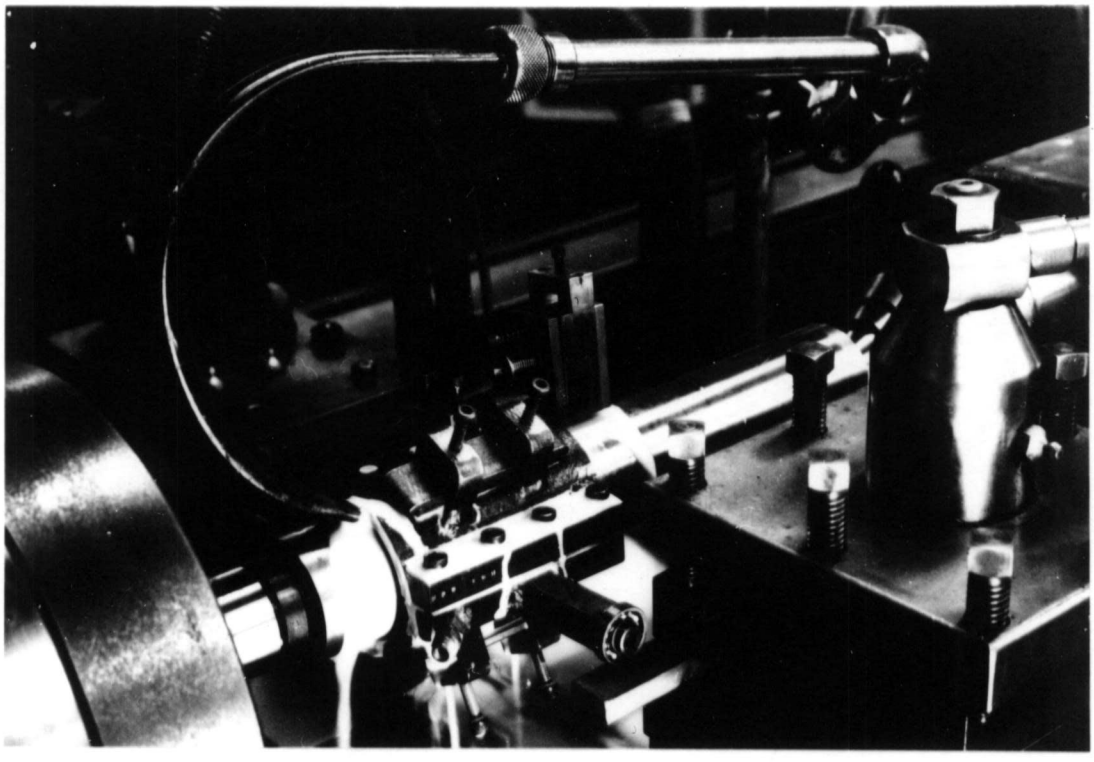

Fig. 5. Merton Nut in use.

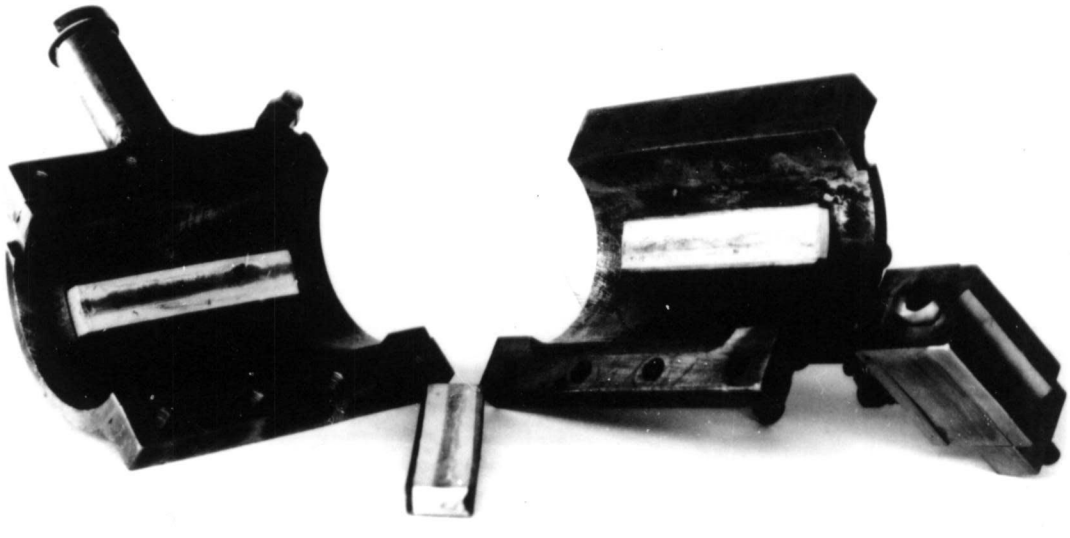

Fig. 6. Merton Nut split open to show Pads.

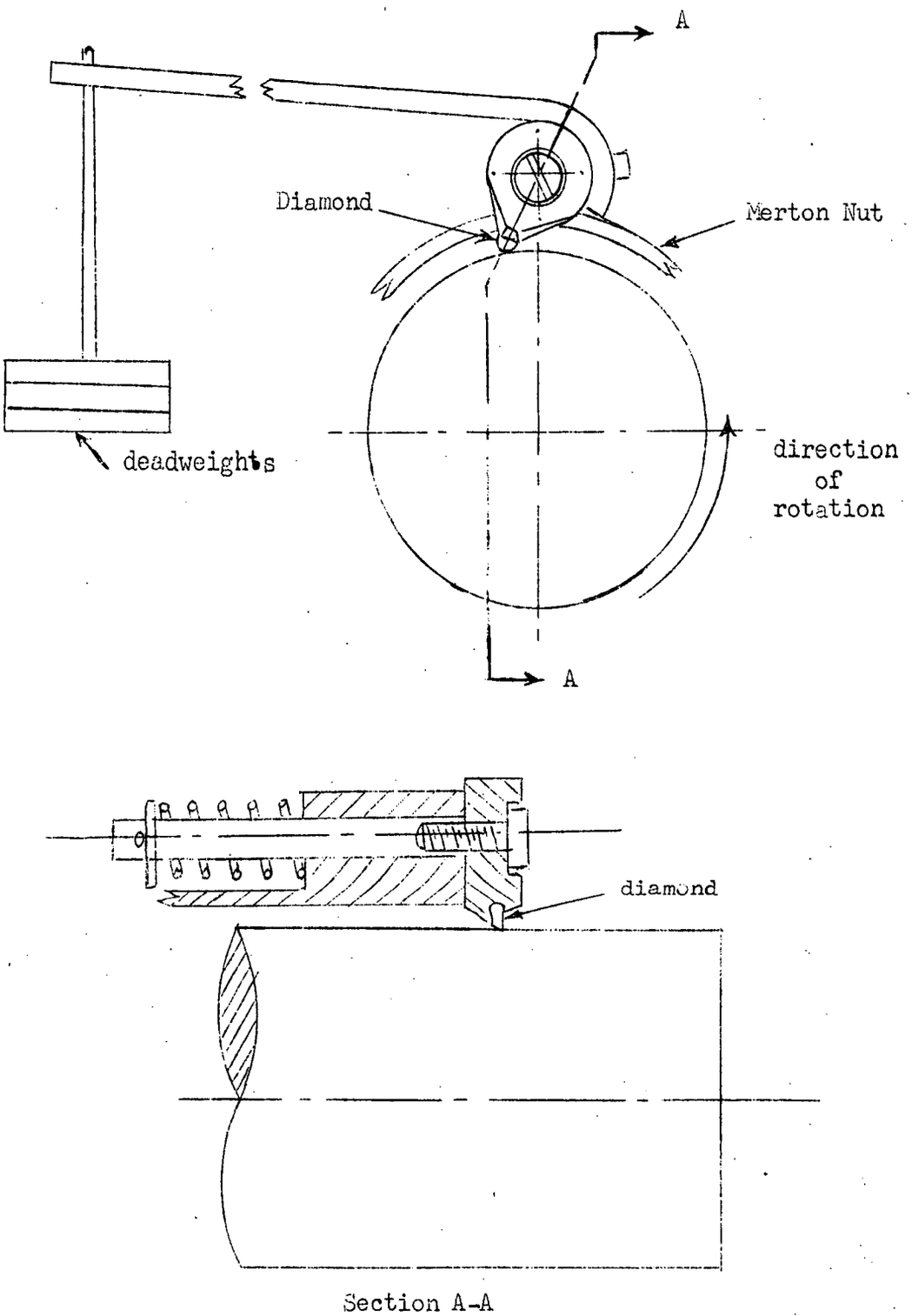

Fig. 7. STU/F5 Diamond Tool and Holder.

The tool and its mounting underwent considerable modification during the course of the investigations. Initially high speed tool steel and tungsten carbide tools were tried. However the remarks made in the previous section also apply here. Gratings produced with these tools lacked the brilliance and dispersion of those made later using diamond tools, and moire fringes were visible only in the zero order.

The first diamond tipped tool used was a Triefus * STU/F5, a faceted turning tool with no rake and a 6° clearance angle. This tool was mounted on edge and held against the work with a force of 2-3 lbs by a system of deadweights, as shown in fig. 7. This tool was expected to form the groove by a squeezing action, as in the normal Merton - N.P.L. process, but in spite of the high negative rake large quantities of turnings were produced, indicating that the tool was, in fact, cutting.

This system was used to produce a very good 1000 line/inch master grating, but was not entirely satisfactory for the following reasons. Firstly, the deadweight system was somewhat temperamental, working well on some occasions, and at other times showing a tendency to irregular cutting action. Secondly it was feared that the diamond, working in a direction different from that in which it was designed to cut, may wear out too quickly (9). In addition the deadweight system as used had no provision for altering the blaze angle without regrinding the diamond.

The final cutting tool and its holder are shown in figures 6,8. The tool was as Triefus SMS10 parting and grooving tool. As can be seen in the figure the tool was held rigidly against the work by a set screw, and could be rotated in either of two planes. The tool was selected from a batch to have a corner radius less than 0.0001 inches. This tool and its mounting has cut a grating of 3000 lines/inch with good results, but further improvements appear necessary to enable gratings of 6000 lines/in and finer to be made.

2.2.3 Use of the Merton Nut

Before using the Merton Nut the rubbing faces of the Ulon Pine pads were given a light rub on a strip of emery paper,

---

* Triefus is a trade name.

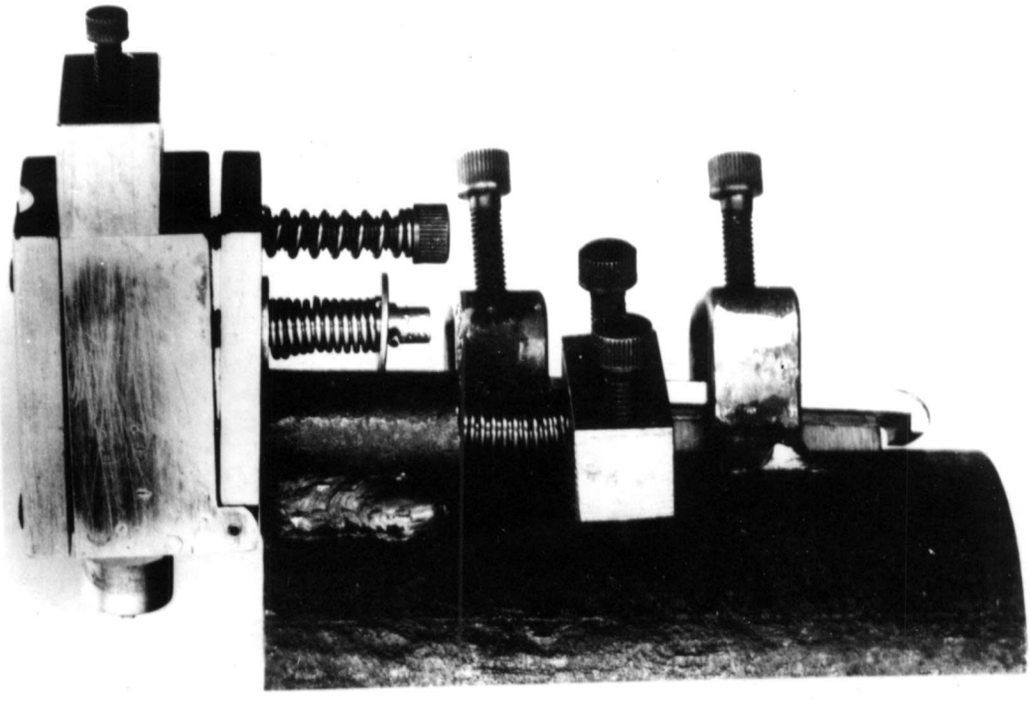

Fig. 8. SMS10 Diamond Tool and Holder.

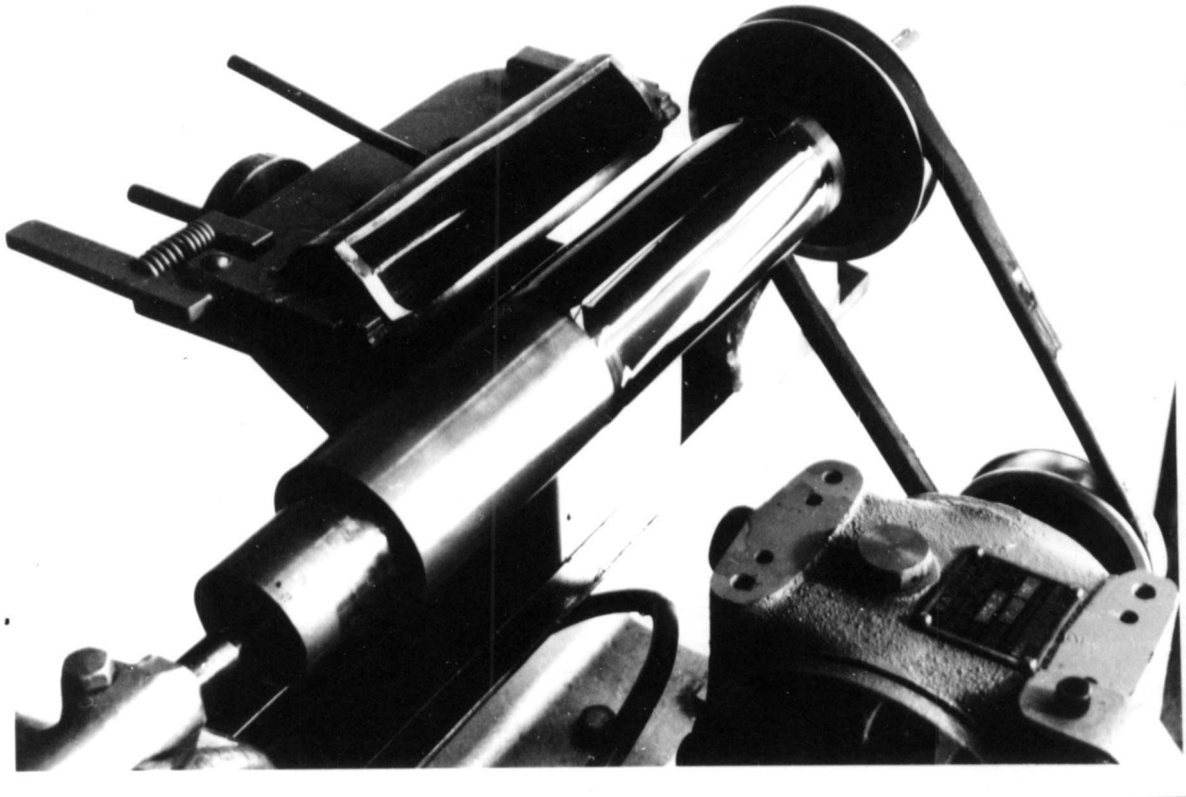

Fig. 9. Apparatus for Pouring Replicas.

and P.T.F.E. tape glued on with Eastman 910 Cement. The nut was then bolted over the cylinder and the pads clamped down firmly. The lathe was run at a speed of 47 r.p.m. while a full flow of coolant was applied as shown in fig. 5 in order to provide extra lubricant for the nut, as well as for cooling and to wash away the swarf.

Some skill and patience was necessary with the nut. On occasions it did not move at all; on others it moved too quickly, or even backwards. However once it had locked onto the driving thread no further troubles were experienced. Sometimes a shorter bar was used to support the arm which prevents the nut from turning and the rack feed was engaged. A sponge rubber pad between this arm and the toolpost was then used to encourage the nut to lock onto the thread. This pad was, however, used only for the first $\frac{1}{8}$" of the helix.

2.3 The Grating Replicas

2.3.1 The Solution

The solutions from which the replicas were made consisted of polymethyl methacrylate dissolved in methyl ethyl ketone with a small quantity of di-butyl phthalate as a plasticiser to aid in the stripping process. The solutions were of two different types depending upon the source of the polymer, which was either "Perspex" * shavings (made by cutting Perspex sheets in a milling machine) or "Diakon" + moulding powder. Presumably because of the differing molecular weights of these two polymers, differing proportions of solvent were required as follows:

---

* "Perspex" is the trade name for polymethyl-methacrylate sheet and tubing as marketed by I.C.I. - other trade names are "Plexiglass" and Lucite".

+ "Diakon" is the trade name for polymethyl methacrylate moulding powder as marketed by I.C.I.

Soln. a)

"Perspex" shavings	10 grms.
methyl ethyl ketone	200 ml
di-butyl phthalate	2 ml

Soln. b)

"Diakon" powder	80 grms
methyl ethyl ketone	180 ml
di-butyl phthalate	2 ml

Thorough mixing of the ingredients was found essential to produce a lump-free mixture - 2½ hours for solution (a) and 4 hours for solution (b) in a mechanical stirrer (with a plain shaft used as the stirring rod) was found to be sufficient. A short period of standing allowed all bubbles to escape, but the solution improved in consistency with 2-3 days standing.

Very little difference was found between the solutions, either in handling or in the finished replicas, the only significant difference being the reduced time required to mix solution (a). However the making of the shavings required for this solution was a time consuming process, and required the use of a scrupulously clean milling machine.

2.3.2 Making the Grating Replicas

Initially the pouring process was carried out in a lathe with an extra reduction gearbox in the drive to give a turning speed of 10 r.p.m., the pouring tray being mounted on the toolpost. However the pouring apparatus shown in fig. 9 was later constructed from an old woodturning lathe. The minimum clearance between the pouring lip of the tray and the grating surface was adjusted by means of a stop on the tray feed screw. This distance was normally set at 0.023", and the finished replicas were then 0.007" thick due to the high shrinkage of the film.

The polymethyl methacrylate solution was poured onto the cylinder during the course of one revolution of the cylinder. The tray was then returned to the horizontal position and the straight pouring lip used to trim the replica for a further revolution, after which the tray was quickly withdrawn and the excess solution returned to the stock bottle. The cylinder was left to rotate until the film was dry.

The drying period varied considerably depending upon the weather conditions and film thickness, but 1 hr. was normally sufficient. On days of high humidity (above about 80%) the replicas tended to take on a frosty appearance upon drying. This was prevented by blowing warm air over the cylinder as it dried.

After drying the cylinder was placed in a drying oven at 85°C for 1 hr. to drive off the last traces of solvent. The grating was then allowed to cool and immersed in distilled water for a further $\frac{1}{2}$ hour. The replica swelled slightly as it absorbed water, and broke free from the master grating. Finally the replica was wiped dry, slit along the axis of the cylinder with a razor blade or sharp knife and peeled off. The replicas were stored flat between sheets of paper until required.

The master grating was cleaned with chloroform when necessary, and in any case after every 4 or 5 replicas were taken.

2.3.3 Gluing the Grating Replicas to Models

Much research was necessary to find a suitable gluing technique to attach the gratings to models. Since the gratings and almost all the models were made from perspex, perspex glues were the obvious choice, and after certain difficulties associated with their use had been overcome these glues were used almost exclusively.

The properties of perspex cements and techniques for their use are fully described elsewhere[58] but a brief summary does not appear out of place here. Perspex cements may be divided into three classes, which are, in order of increasing strength,

(a) pure solvents such as chloroform,

(b) solutions of polymethyl methacrylate dissolved in a solvent,

(c) solutions of polymethyl methacrylate dissolved in its monomer (all-acrylic cement).

All these glues contain a large proportion of a perspex solvent, and the difficulties associated with gluing the grating replicas arise from this fact.

The first gratings produced were 0.003-5" thick. Gratings thicker than this frequently had wrinkled back surfaces, and were at first discarded as unsuitable. However it was later found that the all-acrylic cement (type (c)) would successfully glue gratings provided they were 0.007" thick, and since this cement is gap-filling, and has the same refractive index as Perspex, the irregular back was of no consequence.

After extensive testing the glue finally chosen was Tensol No. 7,* an all-acrylic cold setting cement. This glue was mixed in the manner described by the manufacturers, and all parts of the model adjacent to the grating were masked with polyethylene film attached at the edges with transparent adhesive tape. Excess glue was poured onto the model along a line near one end of the grating position. The grating was then placed in position and the glue squeezed along under the grating by rolling over the grating surface with a rubber squeegee. By this means all bubbles were removed from under the grating. The glue was left to set with a clean sheet of glass on top of the grating to keep it flat.

---

* A Product of I.C.I.

Glues of type (a) and (b) were successfully used, but the results were not as satisfactory as those obtained with the all-acrylic cement. However for gluing these gratings to steel it was necessary to use Tensol No. 50 cement, a cement of type (b).

Other glues were used with some success, Eastman 910 cement and Epimount epoxy mounting medium being the most successful of those tried. Eastman 910 cement was somewhat tricky to use; excess glue was again required to ensure freedom from air bubbles. The Epimount glue was easy to use, but the glue joint was weak. Adequate bond was available to ensure that the grating followed the master, but the grating could be stripped off the model easily. This may, of course, be an advantage in certain circumstances. Both these glues could be used to fasten very thin gratings.

2.4 Characteristics of the Gratings

The blaze angle and tooth form actually achieved by this process is dependent upon so many variable factors that each grating master differs in some respects from the last, and hence it is impossible to obtain the exact performance desired from each grating, even where the pitch is relatively course. The only reliable test of a grating in order to assess its quality for moire fringe work is to place two replicas in the optical bench and observe the fringes, but other tests have been made in an attempt to obtain some basic information on grating quality. The tests which have been made have mostly been limited to gratings from three different masters, and hence few definite conclusions have been reached, but some indication of the factors which are important in grating production has been found.

The three different master gratings which will be discussed in this section can be described as follows:-

Grating A. 1000 lines/inch nominal pitch, cut with a tungsten carbide tool.

Grating B. 1000 lines/inch nominal pitch, cut with a diamond tool (Triefus STU/F5)

Grating C. 3000 lines/inch nominal pitch, cut with a diamond tool (Triefus SMS10).

As regards their use for moire fringe techniques, grating B gave fringes marginally better than those from grating C, while grating B was very poor.

Observation of the grating replicas after they had been removed from the master gave a good indication of grating quality. Grating B gave replicas through which objects could be seen clearly enough to be recognisable, although these objects exhibit edge colouration and were displaced somewhat from the straight-through position in a direction perpendicular to the grid lines. (This type of observation is incidentally the simplest way of determining the direction of the rulings, and also of checking grating orientation so that two gratings can be placed together with their rulings forming mirror images of each other). A light filament or similar source viewed at a distance through grating B replicas caused brightly coloured spots in several orders. Grating C replicas were very similar, but grating A replicas were not so transparent, objects being only dimly visible, and not suffering any apparent displacement. There were virtually no colour effects at all produced by these gratings ,i.e. their dispersion was very poor. The surface finish was also markedly inferior to those of the other two gratings.

Gratings from any master which had been poured under conditions of high humidity exhibited a foggy or frosted appearance. The brilliance of the colour from these was markedly reduced; presumably the diffusion of the light reduced the collimation of the incident light. Gratings of this type, even when from grating master B or C generally produced moire fringes of low contrast, but occasionally a grating of this type would produce fringes with good contrast. This effect was not common, but indicates that no replica which gives reasonable dispersion should be discarded until it has been tried with a large number of replicas from the same master. It also indicates that there can be some variation between replicas which has a large bearing upon the fringe quality.

In order to examine qualitatively the relationship between groove form and fringe quality, microscopic examination of the grating surfaces was made by means of a metallurgical microscope. Photomicrographs of the grating surfaces of replicas from gratings A, B and C are shown in fig. 10. These photomicrographs show that groove quality is very important. Grating B has the most regular groove form. Grating C is poorer in this respect, but the effect is somewhat exaggerated in this photo since the magnification is 4X that of the others. Grating A is very much poorer than the other two, and indicates that the tungsten carbide tool had something of an irregular tearing action.

Microscopic examination of cross-sections of grating replicas from gratings B and C was also undertaken. Gratings were mounted in a metallurgical mounting medium (Epimount) and ground and polished in the normal manner. (A very light final polish on a diamond lap was all that the gratings would stand without the grating showing a tendency to flow and distort).

A photomicrograph of a cross section of a grating B replica is shown in fig. 11. (The replica occupies the lower right hand half of the photograph). Burrs at the groove corners of the master are in evidence from this section, and are presumably due to the partial squeezing action of the tool used to produce this grating master. Burrs of this type were not shown on grating C replicas, and the groove edges were not as steep.

As a final test of grating quality the gratings were placed in a spectroscope and the spectrum produced by the mercury green line was observed (wavelength 5461 angstroms produced by filtering mercury light through a Wratten 77 filter). The spectrum produced by replicas of grating B is shown in fig. 12, in which the zero order is shown by an arrow. This spectrum exhibits some ghosting, and the lines are not sharp enough for serious spectroscopic work. However the spectrum does exhibit two strong orders (the 1st and 2nd), one somewhat weaker order (the 3rd) and several other still weaker orders. Grating C exhibited a more complex pattern of order intensities; one strong order(+1) two somewhat weaker (zero and -1) followed by the two other orders (+2 and -2), with a few still weaker orders visible. C also shows more ghosts than B.

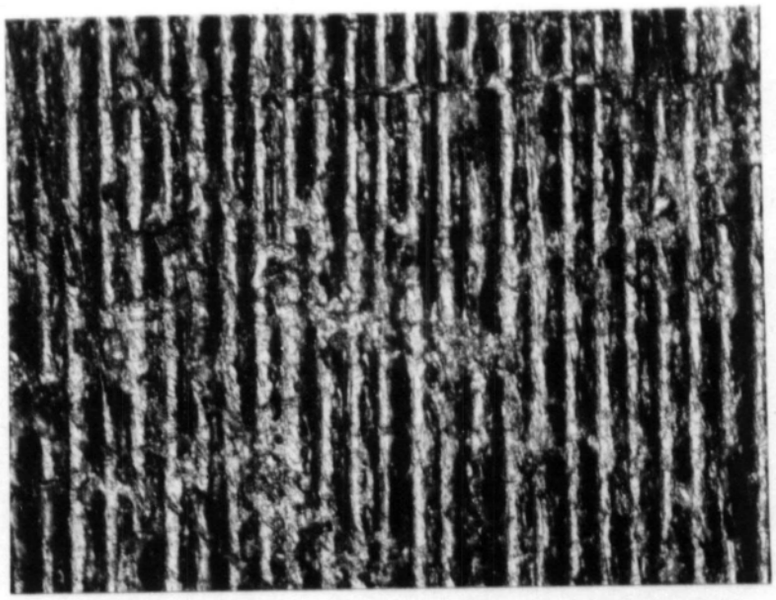

a. 1000 lines/inch, cut with tungsten carbide tool

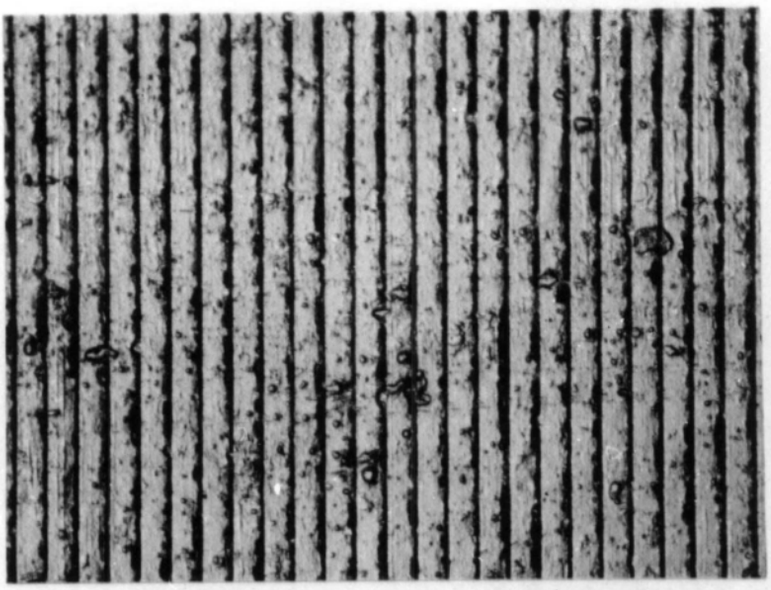

b. 1000 lines/inch, cut with diamond tool.

c. 3000 lines/inch, cut with diamond tool.

Fig. 10. PHOTOMICROGRAPHS OF SOME GRATINGS

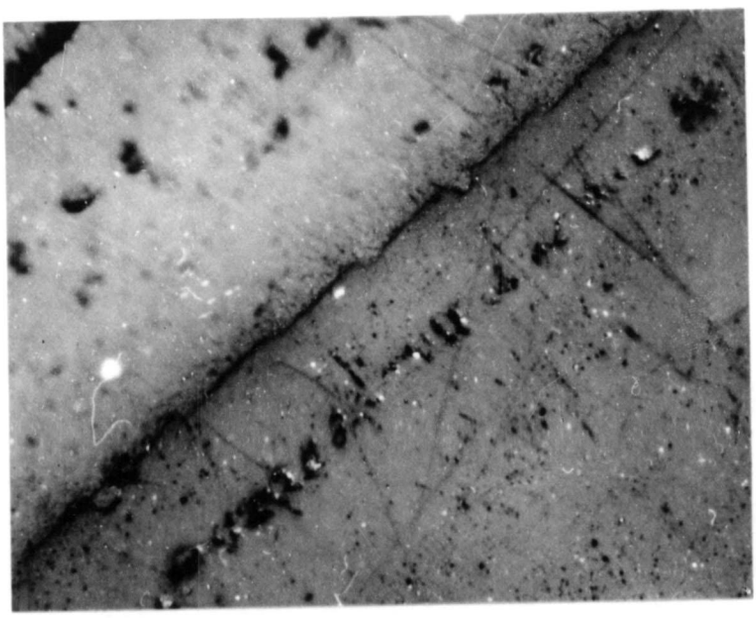

Fig. 11. Photomicrograph of a Grating Cross-section.

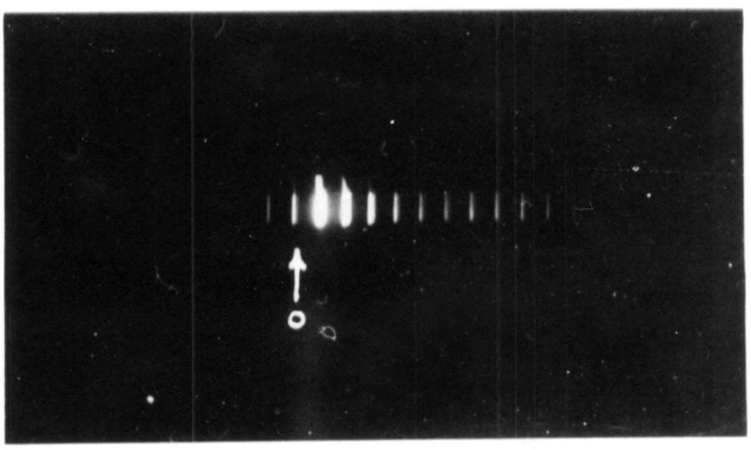

Fig. 12. Spectrum Produced by a Grating.

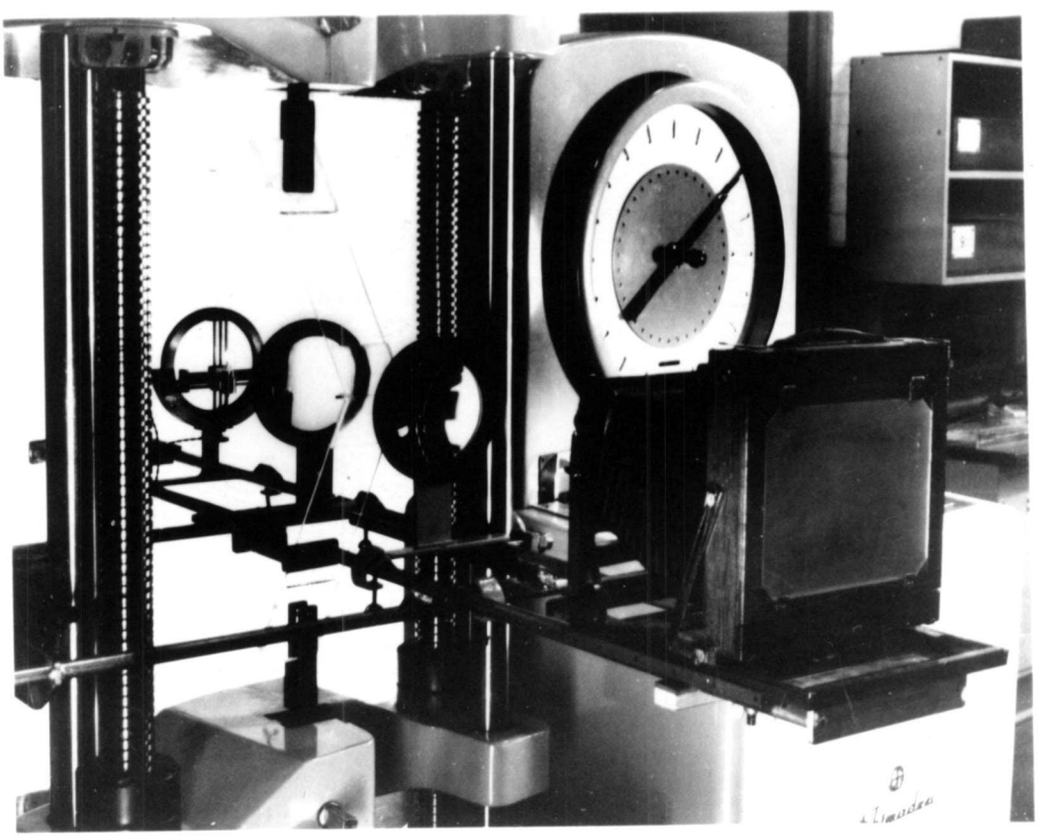

Fig. 13. Test Rig for Knee Joint.

3. Experimental Technique

3.1 The Optical Bench

The optical system for viewing fringes is shown in fig. 13a. The light is passed through a slit and then collimated by means of the collimator lens. After passing through the gratings the light is collected by the field lens and focused onto a second slit. When monochromatic light is used for illumination this slit can be reasonably large - it merely acts as a stop to select one order in which to view the fringes. However it is usual in moire fringe applications to use the second slit as a monochromator slit, allowing the use of a white light source. A lamp with a fine, straight filament, such as an exciter lamp can then be used and the collimator slit dispensed with.

The optical bench and testing machine used for the knee joint tests are shown in fig. 13. The testing machine was a Shimadzu hydraulically operated universal testing machine. In the 0-1000 lb. range this machine was capable of reproducing loadings within 1-lb. in the range 10-200 lbs. The machine was calibrated by placing deadweights on the lower platen.

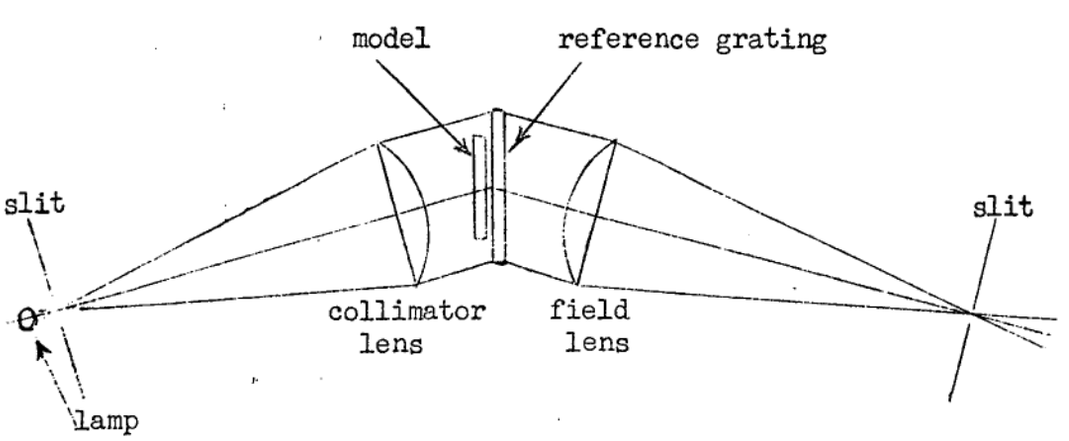

Fig. 13a. Optical System for Viewing Moire Fringes

The light source was a 6 volt 1 amp exciter lamp with a 4 x $\frac{1}{4}$mm. filament. The holder (see fig. 13) was designed so that the lamp could be translated in the directions parallel and perpendicular to the filament, and could be rotated through 360° about the optic axis of the system. Lamps were run at reduced voltage (3-5 volts) to allow the filament to operate in any orientation while still obtaining useful life from the lamp.

Collimator and field lenses were both single plano-convex condenser lenses $5\frac{1}{2}$ inches in diameter and with a $10\frac{1}{2}$ inch focal length. The camera used was a half-plate studio type camera with air bulb release. The lens and shutter system of this camera could be moved in any direction and, being large and of the symmetrical type, the lens could be easily dismantled to allow the slit (cut from stiff black paper) to be inserted against the iris diaphragm. Ground glass focusing was used, and the large format allowed full-size photographs to be taken.

Two methods of mounting the reference grating in close proximity with the model grating have been used. In the first of these methods the grating was mounted on an adjustable bracket attached to the optical bench. This mounting allowed easy adjustment of the reference grating and simplified qualitative study of the effect of air gap on fringe contrast. However this type of grid mounting was not satisfactory in all cases. The knee model deformed sufficiently to cause the joint to move about $\frac{1}{8}$" during loading and hence for measurements after the flanges had been glued in place an alternative method was necessary. A second disadvantage was that the models generally underwent some rigid body rotation. This rotation, if too large, can mask the essential form of the displacement curves, although, since this is a type of rotational mismatch (48), it may improve the accuracy of measurement of the shear strains (provided the amount of rotation is the same for the u and v measurements, or can be measured separately).

The method of mounting the grid adopted in cases where the bench mounting was unsuitable was to clamp the reference to the model by various means. The detail of the clamping method varied from model to model, and will be described where the model tests and results are described (pages 59,61) Obviously the clamping must be such that the reference grating does not place a restraint on the model, nor should it suffer deformation during loading. Where possible the reference grating was fixed along a line of symmetry of the model, since lines of symmetry suffer no normal or shear deformations, and were generally chosen as axes for the frame of reference.

Because of the optical system used, the poor quality of the lenses, and the fact that the system was used off axis, a small amount of pincushion distortion and curvature of field were evident. Other monochromatic aberrations were doubtless also present, but their effect was not evident, and because essentially monochromatic light was used, chromatic aberrations had no effect. Sufficient depth-of-field was present to accommodate most of the field curvature, but improvement was occasionally possible by tilting the camera back. The distortion could not be eliminated, so a grid was normally ruled on the model surface with a sharp scriber or with a pantograph engraving machine. These rulings were filled with indian ink to allow them to remain visible after the gratings had been glued in place. (Alternatively the rulings could be scribed after the gratings were in place, or merely drawn on with indian ink).

The bench was set up and adjusted by the following method.

1. The collimating lens and light source were adjusted to give collimated light. This was done by using a Tuckermann strain gauge autocollimator mounted on a V-block type support. The lamp was run at 1 volt, and its position varied until its coils could be seen sharply focused on the autocollimator graticule.

2. The model, reference grating, field lens and camera were placed in psoition and the lamp voltage was increased to 5 volts. The lamp was adjusted until its filament was parallel to the grating rulings.

The gratings were aligned with their surfaces parallel, and the air gap made as thin as is practicable. The better the collimation, the wider this gap can be, but in any case the contrast improves as the gap decreases. On the other hand the gratings should not be in actual contact. Gratings should also be aligned so that both gratings diffract the light in the same sense; i.e. the grating rulings should be aligned so as to be mirror images of each other.

3. The spectrum from the grating was brought to focus on a piece of white paper placed against the iris diaphragm of the camera lens system while only the front lens was in place. The slit was then placed in the camera parallel to the grating rulings, the back lens of the lens system was replaced, and themodel brought to focus by adjusting the ground glass screen.

4. The size of the image was varied by adjusting the field lens and repeating the sequence 3.

5. The spectral order in which viewing and photography were to take place was selected by moving the camera lens (and hence the slit) and finally the system was adjusted for minimum deviation. The check for this (6) is to slide a microscope cover slip (or a microscope slide in the case of course gratings) in between the gratings. Significant errors in alignment show up as discontinuities where the fringes cross the boundaries of the glass.

3.2 Viewing and Photographing the Fringes

3.2.1 Mismatch

The gratings produced by the process described show remarkably even pitch across the grating surface, but in general pitch variations between gratings of up to 1% are possible. If a number of reference gratings are available, choosing matched pairs may be possible, but normally one fringe/inch is the best match that can be achieved. Furthermore the gratings may exhibit local variations of pitch caused during the gluing process. These local variations rarely reach 0.5%, and hence can have negligible effect on the accuracy of the method, but they do result in poorly defined fringes at wide fringe spacings.

It will be seen, therefore, that the "simple" moire technique (section 1.4.1) can rarely be used. The gratings lend themselves more readily to the mismatch technique (section 1.4.2), which results in greater accuracy in any case. The mismatch technique has been used by the writer on several occasions, particularly to study stress concentrations, but suffers from the disadvantage mentioned before, in that the functional form of the displacement pattern, and hence the deformed shape of the model, is generally not so evident using the mismatch technique. The technique described in the next section allows the use of randomly mismatch gratings to produce the same fringes which would be produced by the simple moire technique.

3.2.2 The Secondary Moire

If a reference grating is placed over the model grid so that a moire pattern is produced, and the model is then loaded, this moire pattern changes. All changes are due to movement of the grating attached to the model. Superimposing photographs of these two moire patterns yields a third moire pattern, and since moire patterns record only changes (at least under the conditions normally encountered in strain analysis - see page 13) this "secondary" moire pattern is the same as would have been obtained in the simple moire technique. (It should be noted that the sharp fringes given by this technique are actually the lines where the displacements are $\pm \frac{1}{2}$, $1\frac{1}{2}$, $2\frac{1}{2}$ etc. grating pitches).

The method described above produces fringes which are generally somewhat sharper than those produced by other methods. Furthermore the averaging effect of the moire pattern has been used twice, allowing the use of poorer gratings than would otherwise be possible (see fig. 14).

A simple mathematical illustration of the validity of the technique used can be given provided once again that we restrict ourselves to small rotations (as are usual in stress problems) to exclude the possibility of obtaining an additive moire.

Referring once again to fig. 3a (page 14) we note that the networks of lines represented by the equations

$$f_1(x, y) = k_1$$
$$f_2(x, y) = k_2 \qquad \text{(v) bis.}$$

cause a moire pattern which is given by

$$F(x, y) = f_1(x, y) - f_2(x, y) = k_1 - k_2 \qquad \text{(vi) bis.}$$

Now let $f_m(x, y) = k_m$ denote the grating lines on the unloaded model,

$f'_m(x, y) = k'_m$ denote the grating lines on the loaded model

and $f_r(x, y) = k_r$ denote the reference grating lines.

Superimposing the loaded and unloaded model gratings would yield the deformation moire pattern

$$F_m(x, y) = f'_m(x, y) - f_m(x, y) = k'_m - k_m. \qquad \text{(xv)}$$

The initial moire produced by the unloaded model and the reference grid is given by

$$F_{mr}(x, y) = f_r(x, y) - f_m(x, y) = k_r - k_m.$$

and the pattern produced by the loaded model and the reference grid is given by

$$F'_{mr}(x, y) = f_r(x, y) - f'_m(x, y) = k_r - k'_m.$$

Superimposing these two moire patterns yields the secondary moire

$$F_s(x, y) = F_{mr}(x, y) - F'_{mr}(x, y)$$

$$= (k - k) - (k_r - k'_m)$$

i.e. $$F_s(x, y) = f'_m(x, y) - f_m(x, y) = k'_m - k_m \qquad \text{(xvi)}$$

thus F_s is identical with F_m and therefore the moire lines represent lines of constant displacement in the direction perpendicular to the reference grid lines.

3.2.3 Photography

The film used for most of the photography was Kodak Royal Pan, which is described as a very fast (400 ASA tungsten) panchromatic film of moderate contrast, medium graininess and with wide exposure and development latitude. This was developed using Kodak DK50 developer in accordance with the manufacturers recommendations. Prints were made on Kodabromide F5 paper, a very high contrast paper. This combination of medium contrast film and high contrast paper appears to give the best secondary moire patterns, but much work could still be done in this field. Because the models normally moved during loading, most of the secondary moire patterns were obtained by superimposing two separate negatives during printing, although double exposure was used on occasion.

The clarity of the secondary moire depends to a certain extent on the number of lines in the initial moire pattern. This was varied by rotating the reference grid, as well as by using reference grids of different pitchs. In most cases about 16 lines/inch in the initial moire gave good results. Near stress concentrations the expected number of secondary lines/inch would sometimes exceed the number there initially, and so the pattern did not appear. In these regions the mismatch technique must be used, and when there are one or two lines/inch in this region initially, the loaded pattern is very close to the true displacement pattern.

3.3 Illustrative Example - Disc with Diametral Compressive Load

In order to test the accuracy of the technique the strains in a disc under a diametral compressive load were measured. It was during these tests that many of the techniques described were developed.

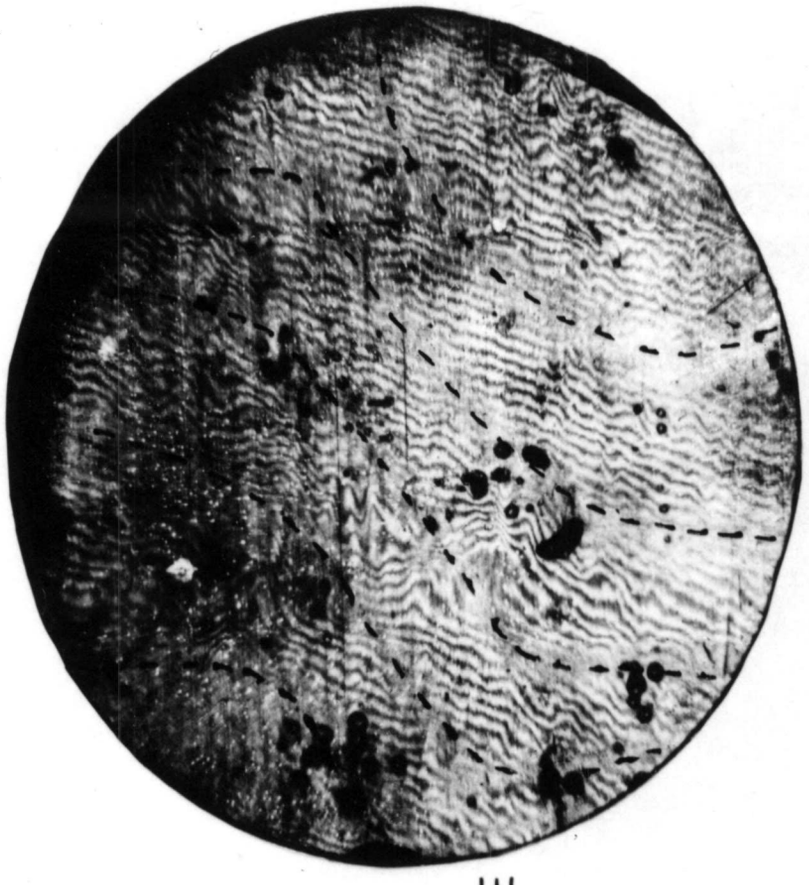

u pattern; grid lines 

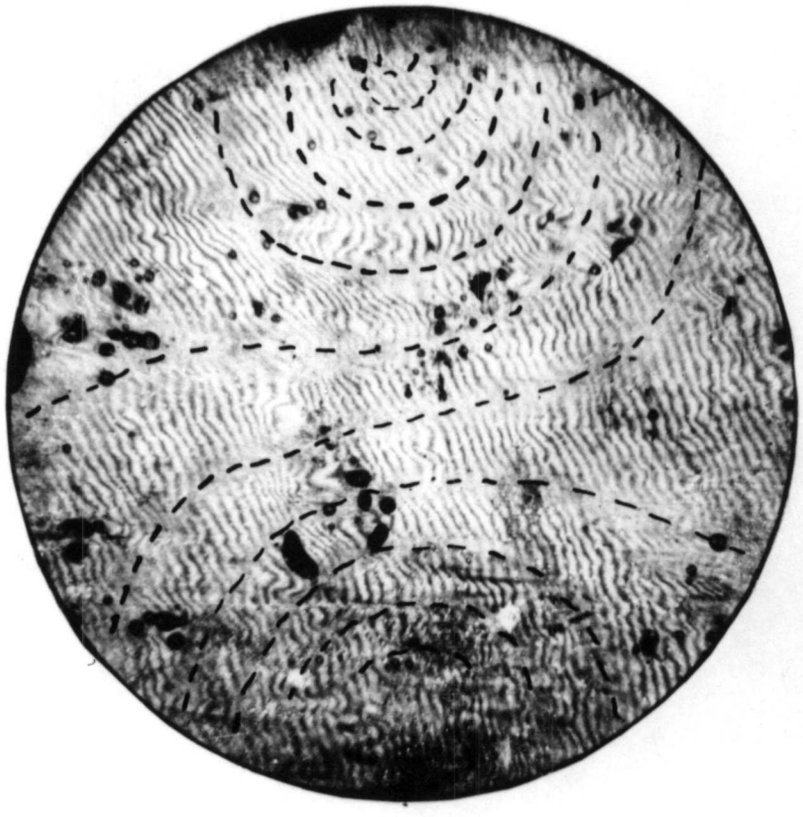

v pattern; grid lines 

Fig. 14. Moire Patterns for Disc.

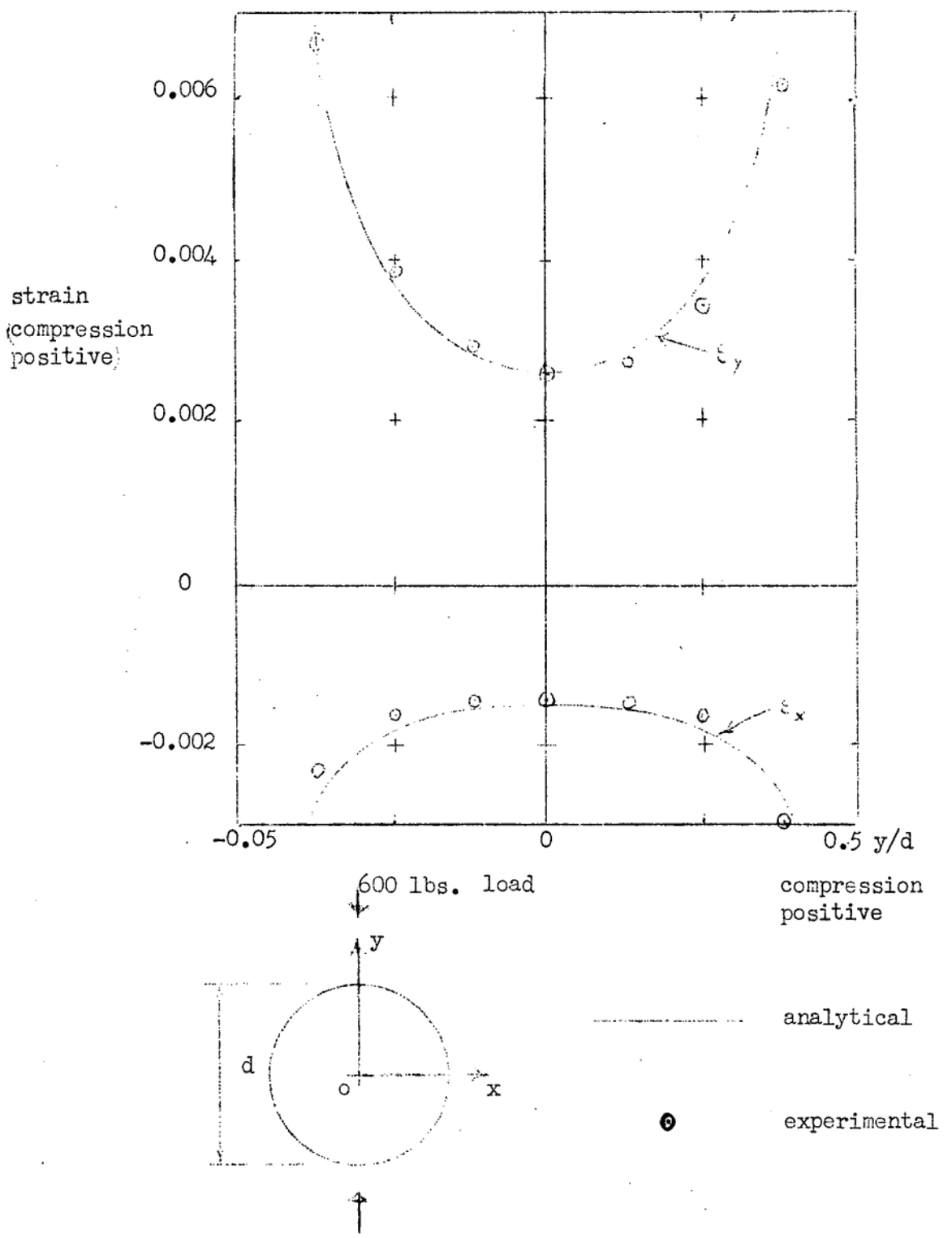

Fig. 15. Strains on Vertical Diameter of Disc.

The disc used for the tests was made from $\frac{1}{4}$" perspex sheet, and was 4.18 inches in diameter. The model grating was only 0.005 inches thick and hence there was much local distortion of the grating. Crazing and bubbles were also present, but the reference grating was very much better in every respect. The disc was loaded in a screw-type testing machine with optical bench attached to the lower (moving) platen.

The light source was originally provided by a fluorescent tube illuminating a variable width slit. The light available through a narrow slit was not large, so slits as wide as $\frac{1}{4}$" were used, and hence the light was not well collimated. Since the light was not split into sharply defined orders no monochromator slit was used, but a type of slit action was achieved by varying the size and position of the iris diaphragm. The photographs shown in fig. 14 were taken by this means, and are included to show how poor the quality of the optical setup can be whilst still obtaining useful fringes. The gratings must, however, be blazed as well as those used; poorly blazed gratings give poor results no matter how good the other optical equipment is.

The obvious defects of the above setup were progressively modified until the type of equipment described in section 3.1 was developed, and this has since been used exclusively. Improved contrast and fringe definition has resulted, and the apparatus is also easier to use and adjust.

Since the movement of the disc during loading was negligible, the double exposure technique was used to obtain the secondary moire patterns. The patterns for a load of 600 lbs. are shown in fig. 14. The effect of rigid body rotations on the displacement patterns can readily be seen from these photographs (c.f. patterns shown in (48)). It should also be noted that the rotation during determination of the u pattern was different from that which occurred during determination of the v pattern, but in this case the existence of two lines of symmetry allowed separate determination of these rotations.

The strains on the vertical diameter calculated from these patterns are shown in fig. 15. Also plotted in fig. 15 are the results of the analytical solution for the strains in a disc (45, 51). The grid pitch used for the experimental results was obtained by direct measurement using a microscope and eyepiece scale. Youngs modulus and Poisson's ratio for the perspex were determined using Huggenberger strain gauges.

The disc experiment has been repeated since using the improved optical setup and grids of 3,000 lines/inch. Photographs and results of this latter test are given elsewhere (59).

4. THE KNEE JOINT

4.1 The Problem and Present Methods of Solution

4.1.1 The Problem

A simple form of knee joint and loading is shown in fig. 16. At some distance from the joint (approx. $\frac{1}{2}$- 1 beam depths) from the joint, and at a similar distance from the load points, the members can be expected to behave approximately as normal beam-columns (principle of St. Venant), but at the joint simple beam theory obviously does not apply. At this joint the flanges impart considerable transverse normal stresses and high shear stresses to the web, and at the same time the flange stresses near the joint are not uniform due to shear lag. Cross-bending of the flanges may also occur.

The problem is normally further complicated by the presence of stiffeners, and by haunching or curving the inner flange to obtain greater depth of section at the knee. Experience has shown that many knees fail because of lateral instability of the compression flange, or by local web buckling. Further stiffening and bracing is therefore usually added to prevent this occurring.

The problem is, in fact, so complicated that many knees are designed "by eye", with only the very roughest of calculations to determine sizes and shapes of component parts. There are, however, some approximate methods of design for the more common knee shapes and these are summarised in the next section.

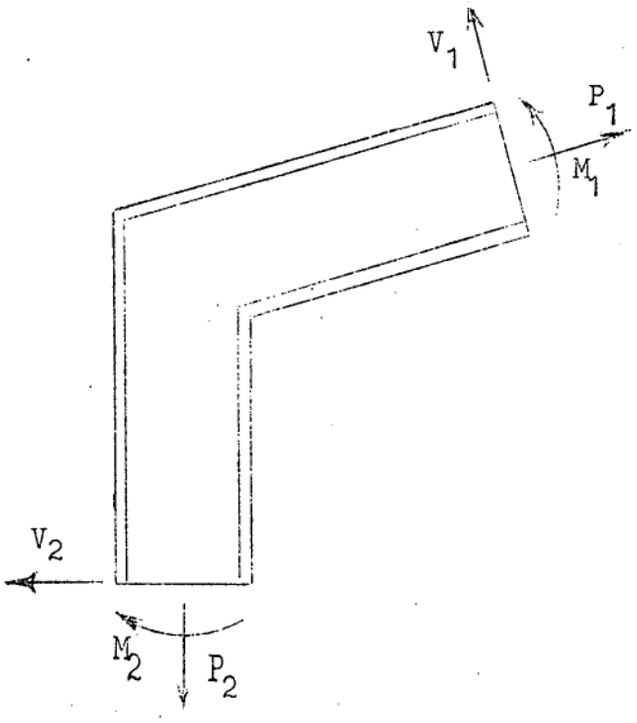

Fig. 16. A Simple Knee Joint.

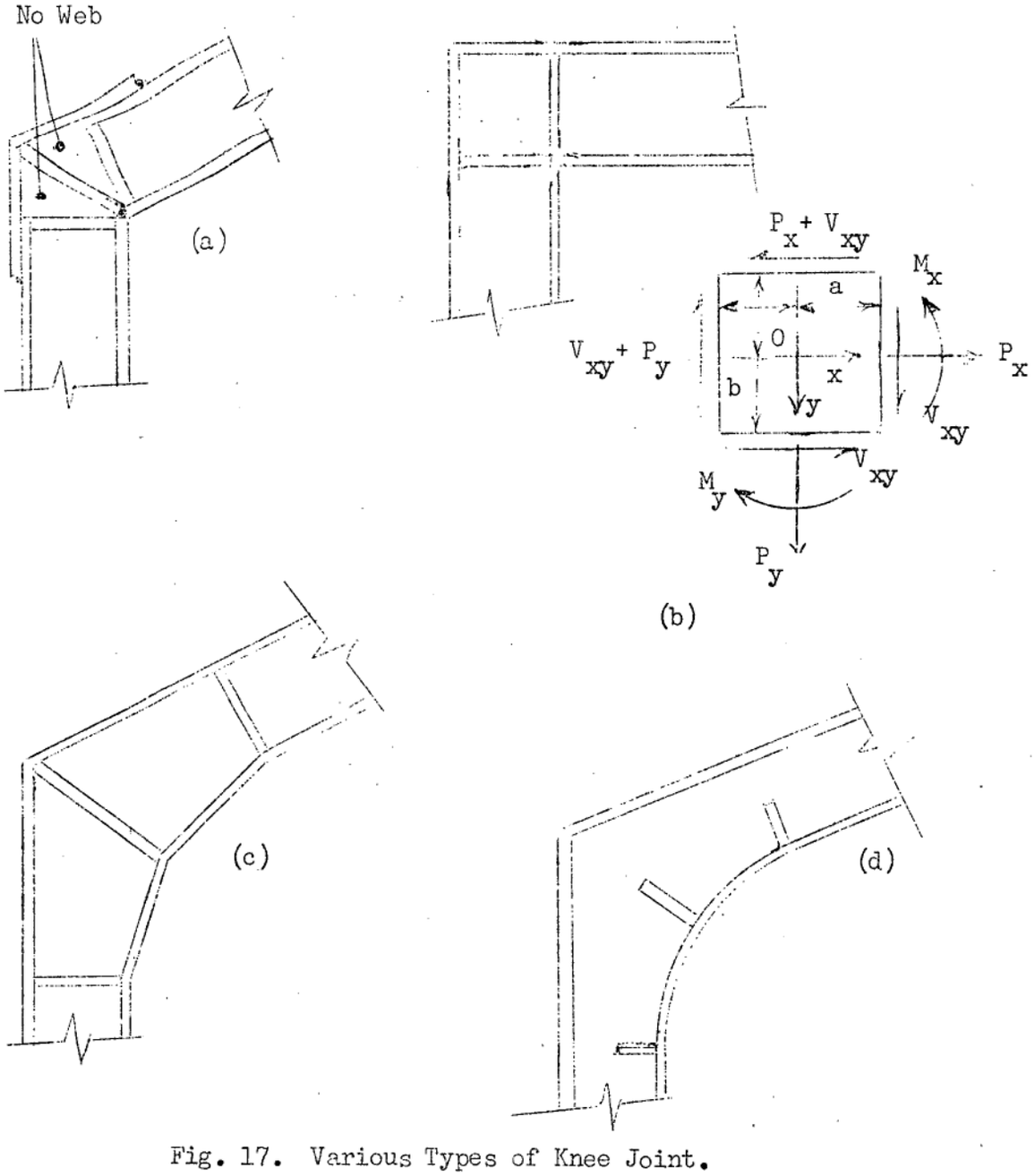

Fig. 17. Various Types of Knee Joint.

4.1.2 Some Methods of Analysis

A summary of the methods commonly used to design knees has been written by Gray et al. (60). Much of our present knowledge of knee joints and similar connections has resulted from the investigations of Hendry (61-63) and from an extensive program of testing carried out at Lehigh University (64-70). Earlier work was carried out at the U.S. National Bureau of Standards (72).

The simplest approach to the design of knee joints is to allow the flanges to take all the bending and axial forces, and the web to take all the shear (60, 66). Where the web is overstressed, stiffeners are added, frequently according to empirical rules due to Hendry (60- 63). As an alternative approach Benjamin, in discussing a paper by Grover (71), suggested omitting the web entirely at the joint, and using a truss-type knee (fig. 17(a)) on the assumption that the behaviour of this type of knee is accurately predictable by present means of analysis.

More complex methods of calculating the stress distribution in the web are available for right-angle knees only. The first of these is apparently due to Osgood (72) and consists of assuming the web at the knee to be a square flat plate loaded by forces and moments in such a way that the edge stresses vary linearly (see fig. 17 (b)). These conditions are satisfied by the Airy stress function.

$$\phi = b_2 xy + \frac{1}{6}(3c_3 + d_4 y)(a + x)y^2 + \frac{1}{6}(3b_3 + b_4 x)(b+y)x^2 \quad \text{(xvii)}$$

It can be shown (60) that

$$b_2 = \left[M_x - a(2V_{xy} + P_y) - \frac{3}{2}(M_x + M_y)\right] / 4abt$$

$$b_3 = P_y / 4abt; \quad c_3 = P_x / 4abt$$

$$b_4 = 3M_y / 4a^3bt \; ; \quad d_4 = 3M_x / 4ab^3t$$

whence

$$\left.\begin{aligned}
\sigma_x &= (P_x + 3M_x y/b^2)/(a + x)\ /4\ abt \\
\sigma_y &= (P_y + 3M_y x/a^2)\ (b + y)\ /4\ abt \\
\tau_{xy} &= -\{M_x - a(2V_{xy} + P_y) + P_y x + P_x y - 3M_y(1-x^2/a^2)/2 \\
&\qquad - 3M_x(1-y^2/b^2)/2\}\ /4abt
\end{aligned}\right\} \quad \text{(xviii)}$$

where

σ_x = normal stress in the x direction

σ_y = " " " y "

τ_{xy} = shear stress on x and y planes

and other symbols are defined by fig. 17(b).

Although this method presumably gives more accurate results than the previous approach, its accuracy is limited by the approximations made in the boundary conditions. Since the computations in this method are somewhat lengthy, Wright (60) has produced the simplified formula

$$\tau_{max} = M_c(\ 1 + a^2t/3Z_a + b^2t/3_Zb)/4abt. \qquad \text{(xix)}$$

where M_c = moment at inside corner of frame

Z_a = section modulus of the column

Z_b = section modulus of the beam

for calculating the maximum shear stress, τ_{max}. A disadvantage of both these formulae is that they apply only to webs of right-angle knees.

Haunched knees and knees with curved flanges (figs. 17c and d) can be approximately analysed by the tapered beam formula due to Vierendeel (60) or by a method due to Olander (60, 73). Knees with curved flanges where the inner and outer flanges are parallel can be analysed with good accuracy by means of the well known Winkler curved beam formula.

The plastic method of design of knees of all forms has been treated in references (60, 63, 65-71 and 74).

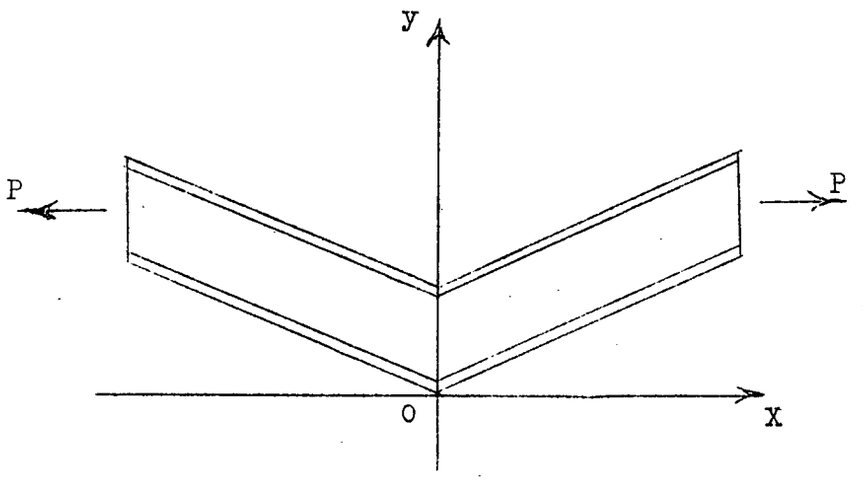

Fig. 18. Symmetrical Knee Joint and Loading System

4.2 Tests of Knee Models

4.2.1 Preliminary Notes

In order to reduce the problem to its simplest terms all knees tested have been of the symmetrical type shown in fig. 18. The line of symmetry of the knee was used as one axis of the coordinate system used for all models as shown in fig.18. The origin of this coordinate system coincides with the external corner of the knee which is a point where all stresses are zero.

As a means of building up an understanding of the overall behaviour of knees, tests were first carried out using knees of rectangular cross-section, and then flanges were added. The next logical step is to add stiffeners before going on to more complex knee shapes and loading patterns, but no work has been undertaken in this direction.

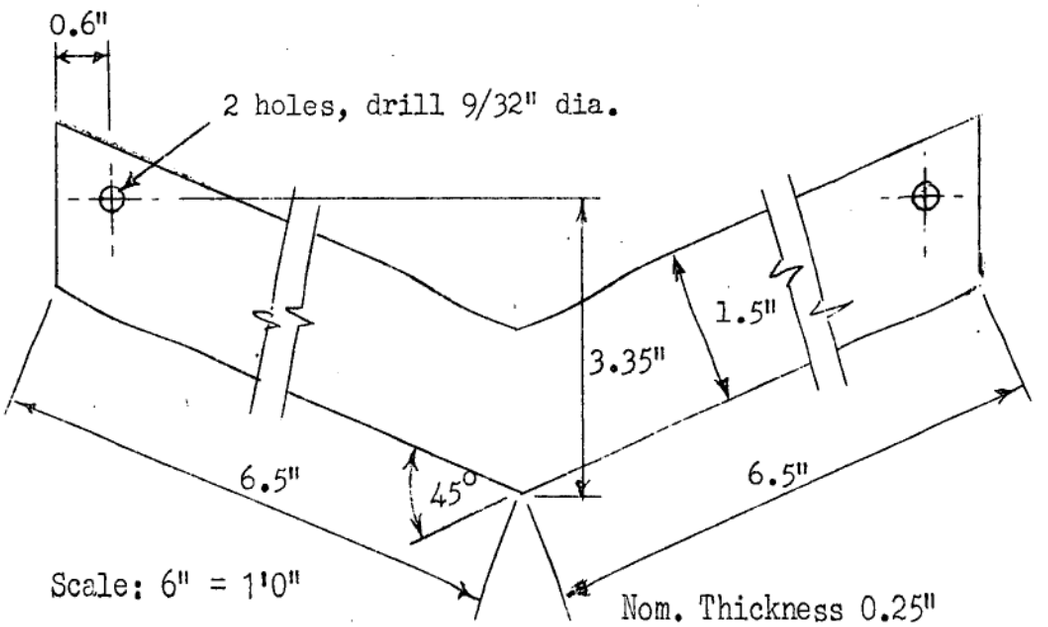

Fig. 19. Small Scale Knee Model.

4.2.2 Small Scale Knee Models with Rectangular Cross Section

The first knee models tested had the dimensions shown in fig. 19. This size was chosen as the largest model which could conveniently be tested in the photoelastic bench available, and to correspond with models of the same dimensions which the author had already tested (75) using conventional photoelastic techniques and the moire method for determining isopachics (20, 23, 24 and 46).

Two identical models were used with gratings parallel and perpendicular to the line of symmetry joining inner and outer corners of the knee. All gratings were nominal 1000 lines/inch grating replicas from master grating B (see section 2.4 p. 34). The reference grating was attached to the optical bench by the bracket described in section 3.1, and the load (57.7 lbs.) was applied by a deadweight and lever system.

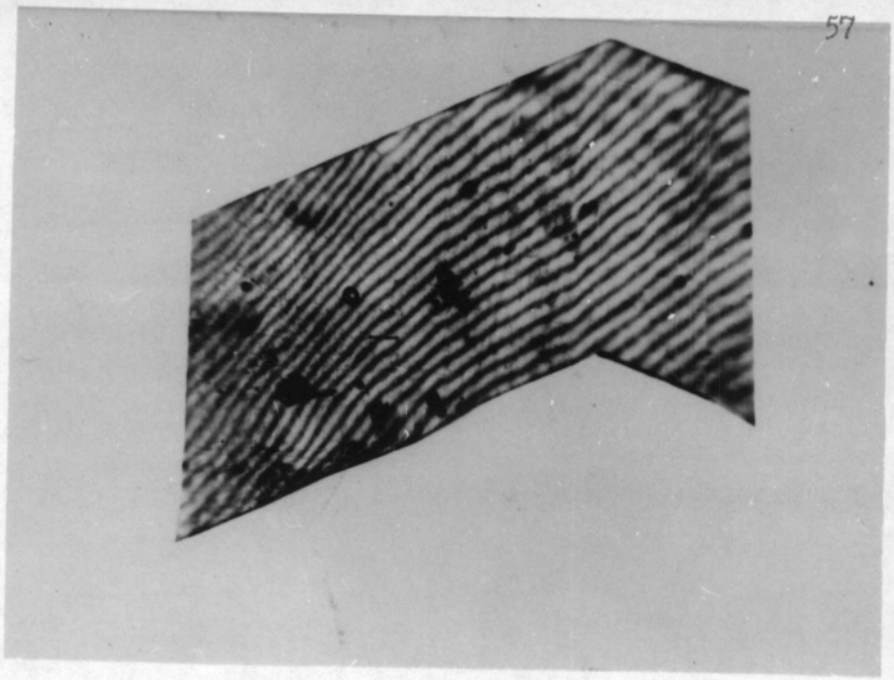

(a) Unloaded Moire Pattern

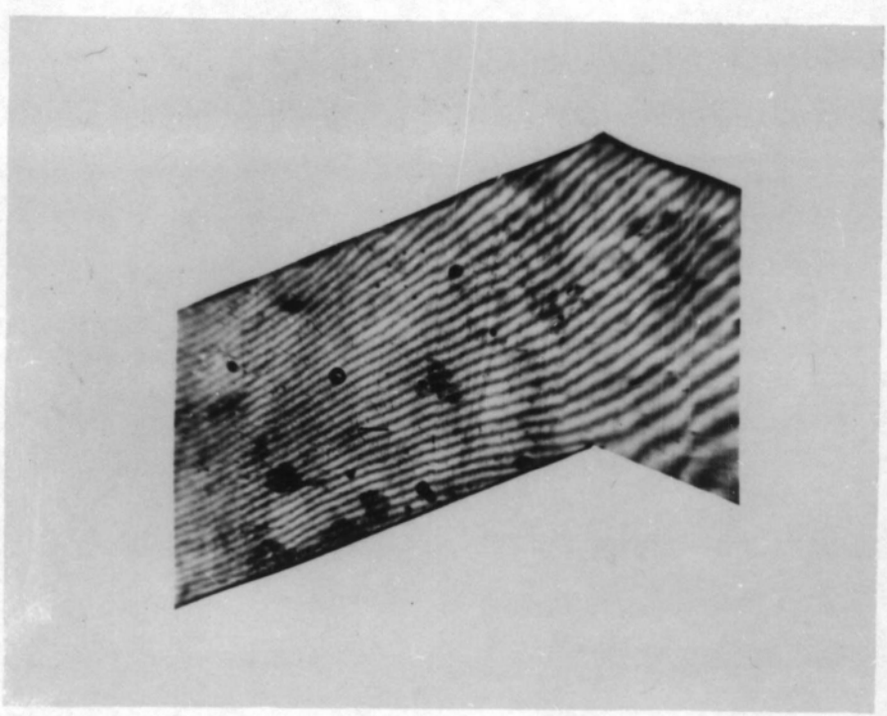

(b) Moire Pattern for 57.7 lbs. Load

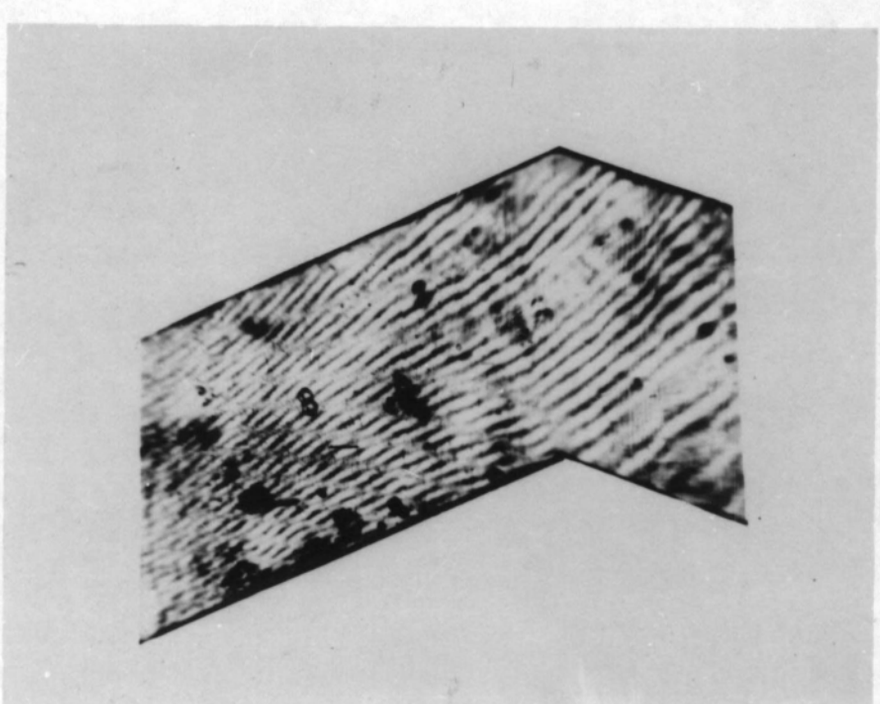

(c) Secondary Moire obtained by Superimposing (a) and (b

Fig. 20. Moire Patterns for Small Scale Rectangular Knee.

Fig. 20 shows the unloaded and loaded moire patterns, and also the secondary moire pattern for the case where the grating lines are parallel to the line of symmetry, i.e. the secondary fringes represent lines of constant u, the displacement in the direction of the x axis. (displacement in the y direction is denoted by v).

It can be seen from fig. 20 that the moire patterns produced are not symmetrical. This was due to the large rotation of the model relative to the loading frame, (approx. $4\frac{1}{2}^{\circ}$). The effect of such rotation was eliminated in later tests by attaching the reference grating to the model at the ends of the line of symmetry. Another fault in the procedure used for this experiment was the lack of a grid scribed on the model to allow strains to be measured accurately in the presence of optical distortion.

The size of model and the bench was altered for later tests because addition of flanges to models of the smaller size was not practical. The glue squeezed from the joint rendered a large proportion of the web unusable. Also flanges stiffened the joint to such an extent that the loading frame would not have been capable of producing sufficient deformation without being overloaded. For these reasons larger models were used in a normal testing machine for all subsequent work.

4.2.3 Large Scale Knee Model with Rectangular Cross Section

Having made the decision to use larger models it was also decided that the faults in the experimental technique noted in the previous section would be rectified by work on this larger scale, rather than by repeating the work already carried out. This also allowed the work on rectangular section knees to be repeated using the gratings

of 3000 lines/inch which had been produced in the meantime, and in any case it was necessary to make a web with gratings attached for experiments on an I section knee.

The dimensions of the knee tested are shown in fig. 21. . A 1" square grid was engraved on one side of the model, and 3000 line/in gratings were stuck on each side of the model to avoid the need for two models. Two separate reference gratings were used, and these were attached to the model in the manner shown in fig. 22(a) The clamping screw had a sharp point so that any transverse deformations would merely cause the point to sink deeper into the perspex rather than restrain the model or deform the reference grating.

The use of orthogonal gratings attached to opposite sides of the same model was very little different from the more usual arrangement of one grating. The light was split up into orders in the two orthogonal directions, and for best results it was necessary to view in the same order in each direction. The light intensity was reduced considerably by the presence of the orthogonal grating, but this was largely counterbalanced by running the lamp at 5 volts instead of the 3 volts which was normally sufficient.

The moire photographs of this large scale knee are shown in fig. 23 and the strains are shown in fig. 26. The load on the model was 51.5 lbs.

4.2.4 I-Section Knee

The final knee tested had I-shaped cross sections and was made by gluing 2" x $\frac{1}{4}$" perspex flanges onto the rectangular section knee described in the previous section (see fig. 21). Moire patterns for the web of this knee at a load of 200 lbs. are shown in fig. 24, and for the external surface of the flanges in fig. 25. Strains are shown in fig. 27.

The method of attaching the reference grids to the model is shown in fig. 22(b). It will be noted from fig. 24 that this method did allow small rotation of the reference grating during loading.

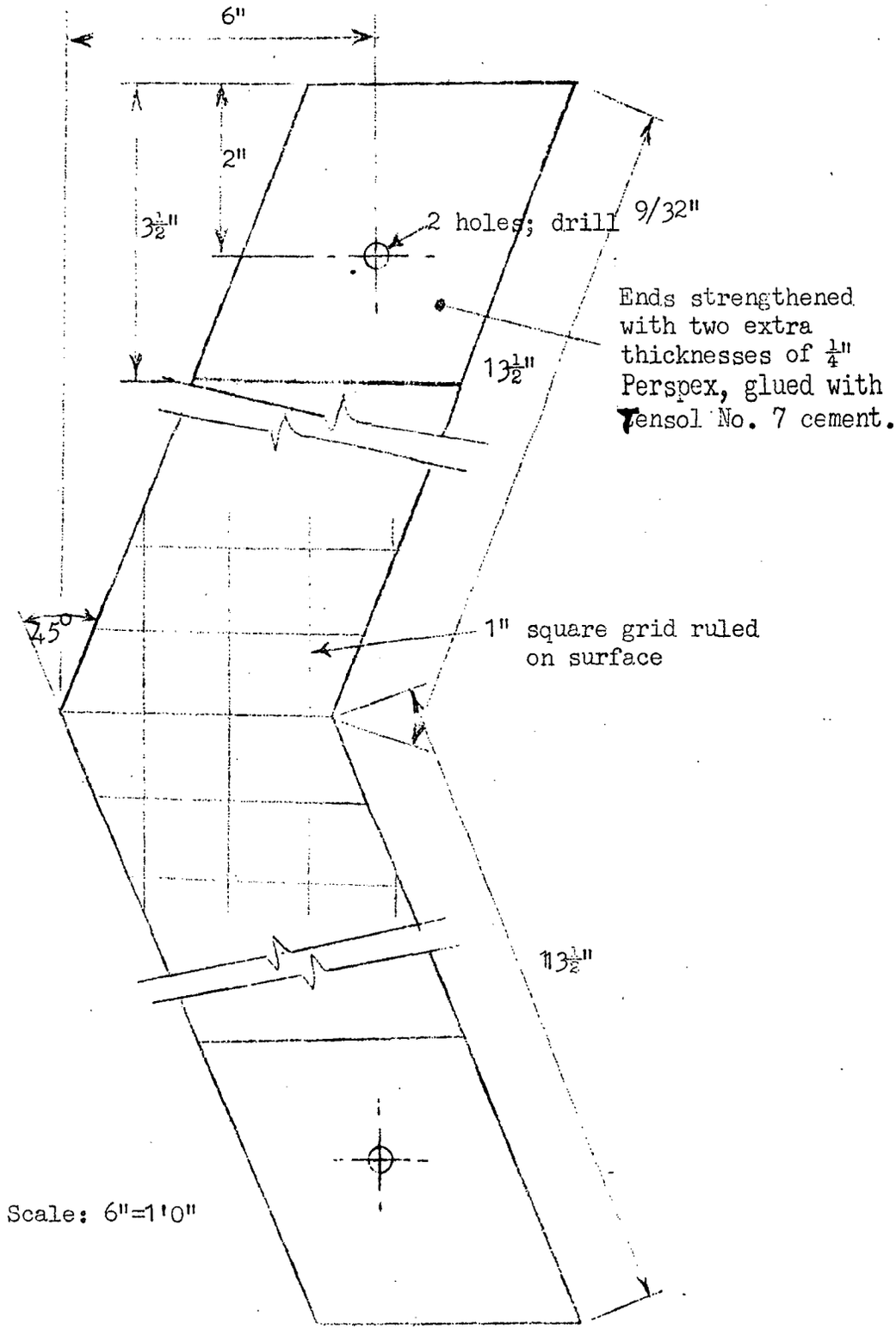

Material: ¼" (nom. thickness) Perspex.

Fig. 21. Large Scale Knee.

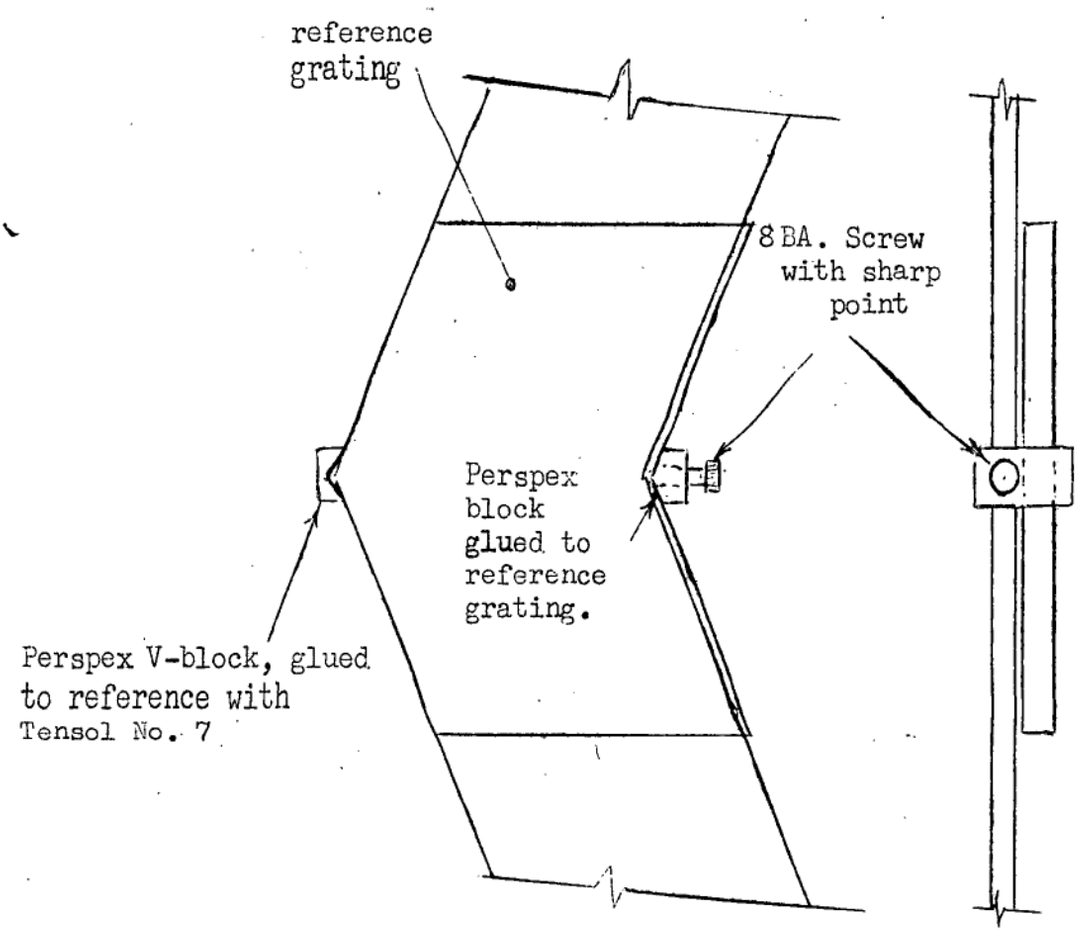

(a) Rectangular Section Knee

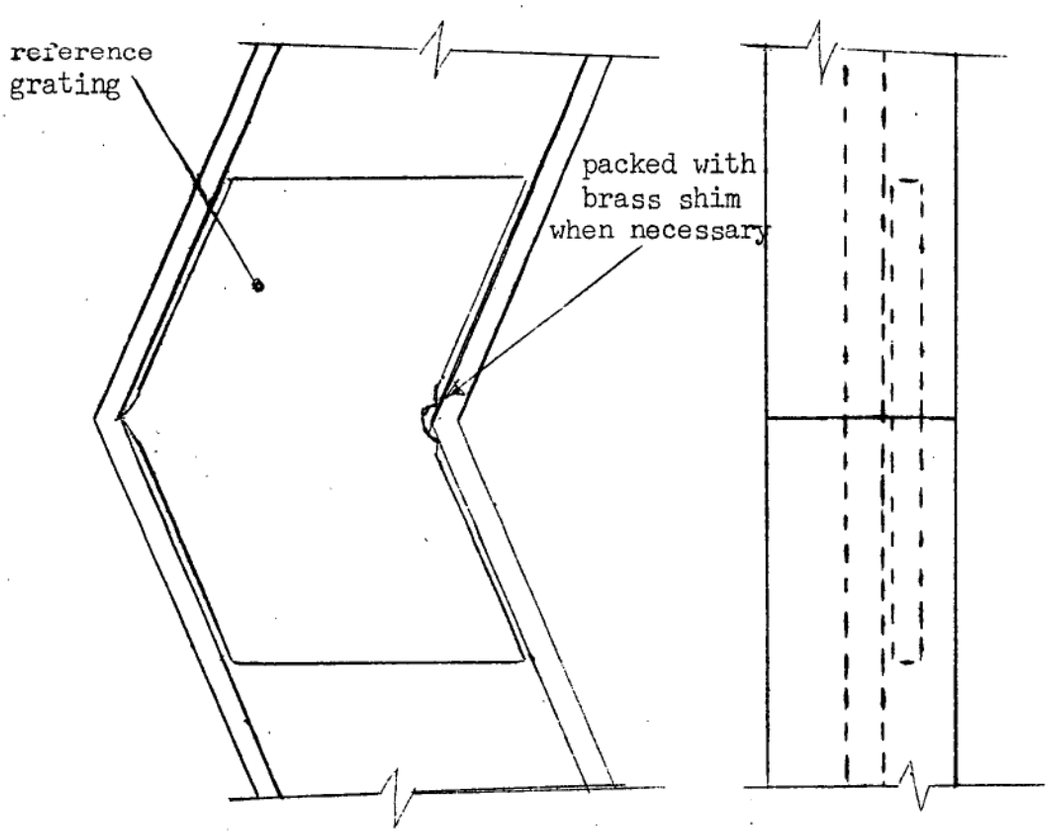

(b) I-Section Knee.

Fig. 22. Methods Used to Attach Reference Gratings to Knee Models.

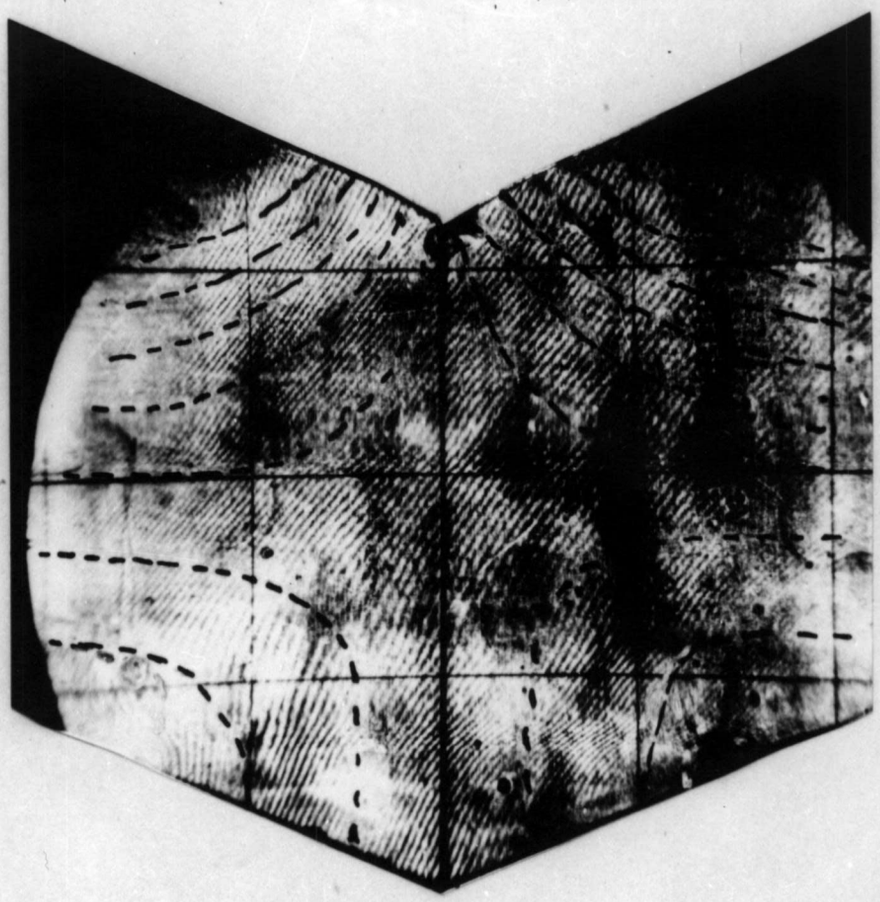

u pattern; grid lines 

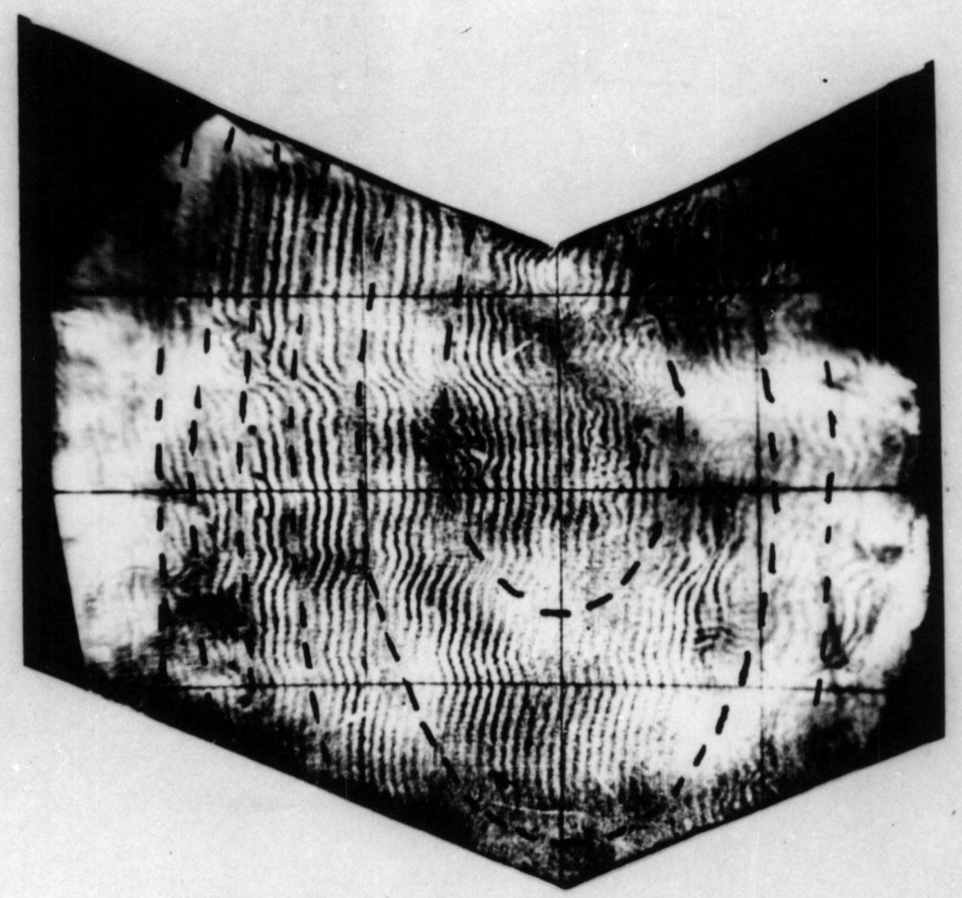

v pattern; grid lines 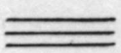

Fig. 23. Moire Patterns for Rectangular Section Knee.

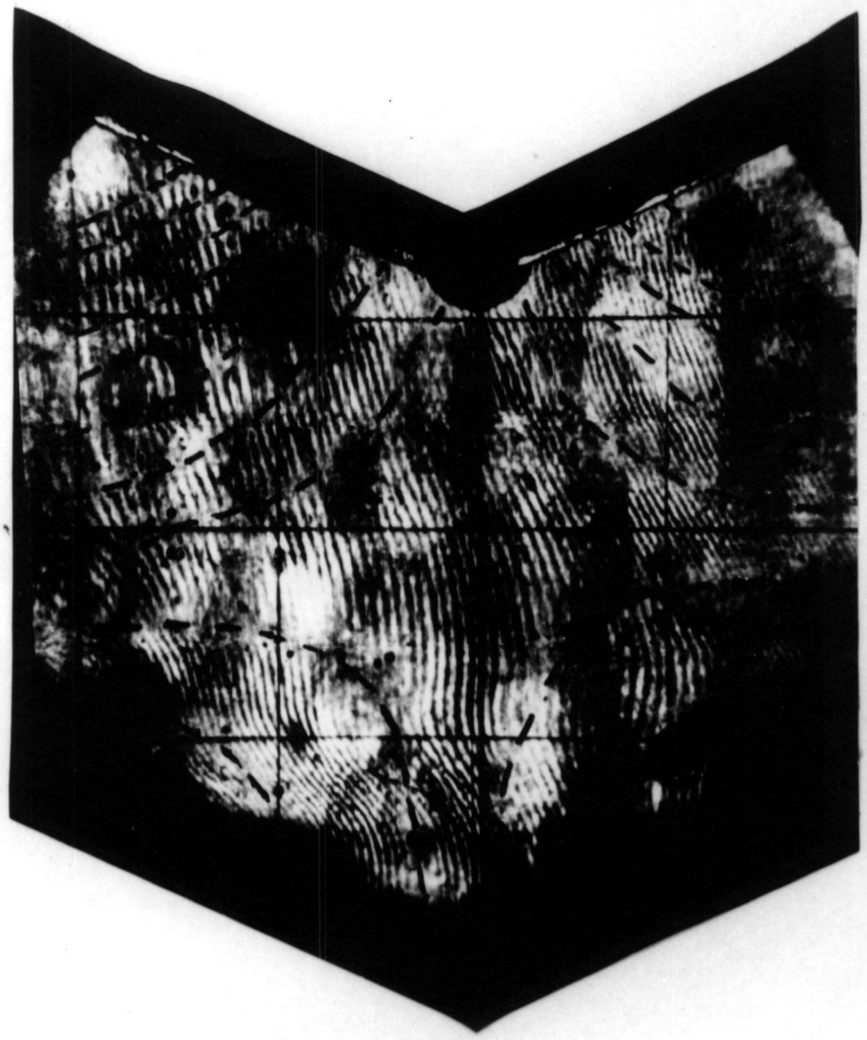

u pattern; grid lines

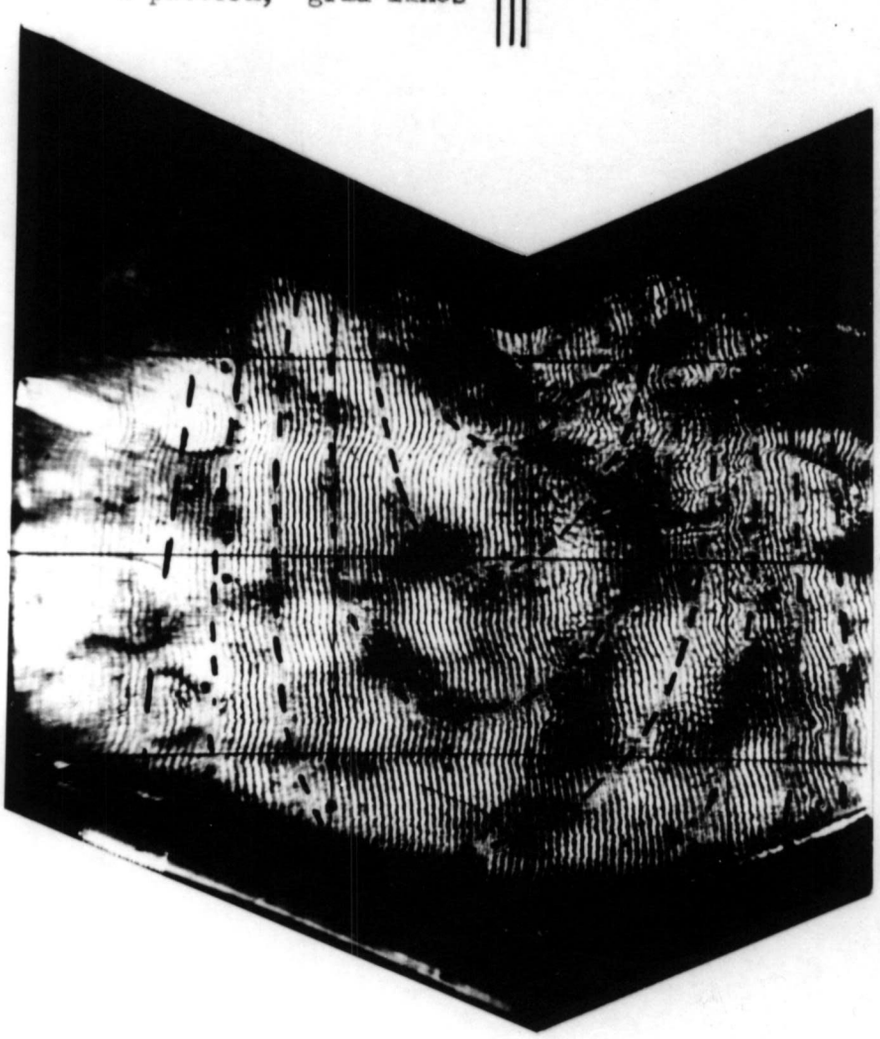

v pattern; grid lines

Fig. 24. Moire Patterns for Web of I-Section Knee.

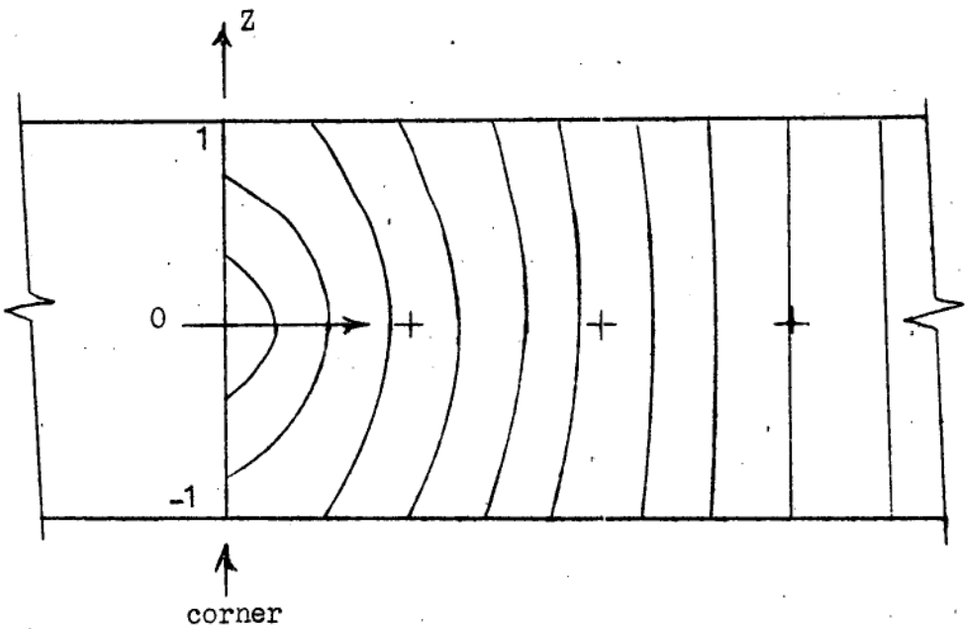

(a) Moire pattern for displacement along internal flange

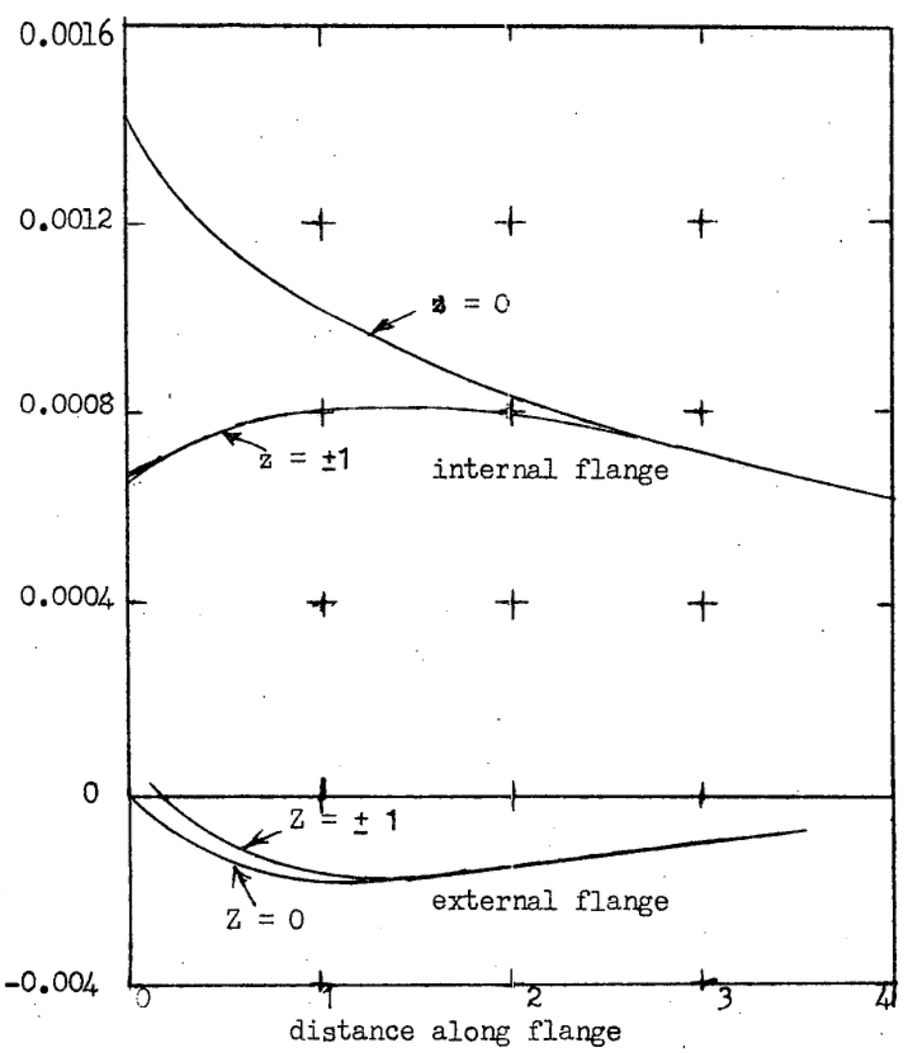

(b) Longitudinal strains on surfaces of flanges

Fig. 25. Moire Pattern and Strains for Flanges of I-section Knee

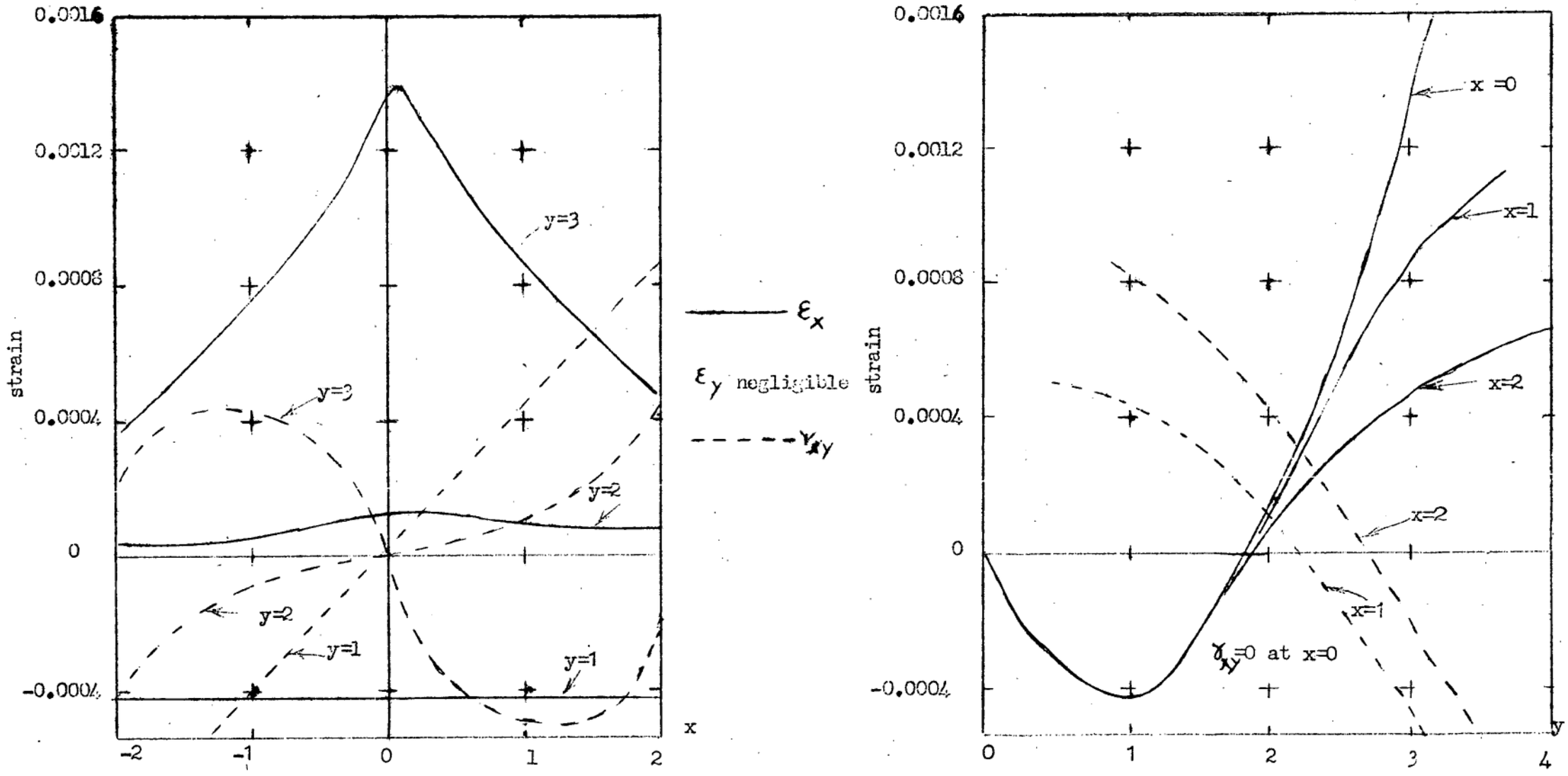

Fig. 26. Strains in Rectangular Section Knee

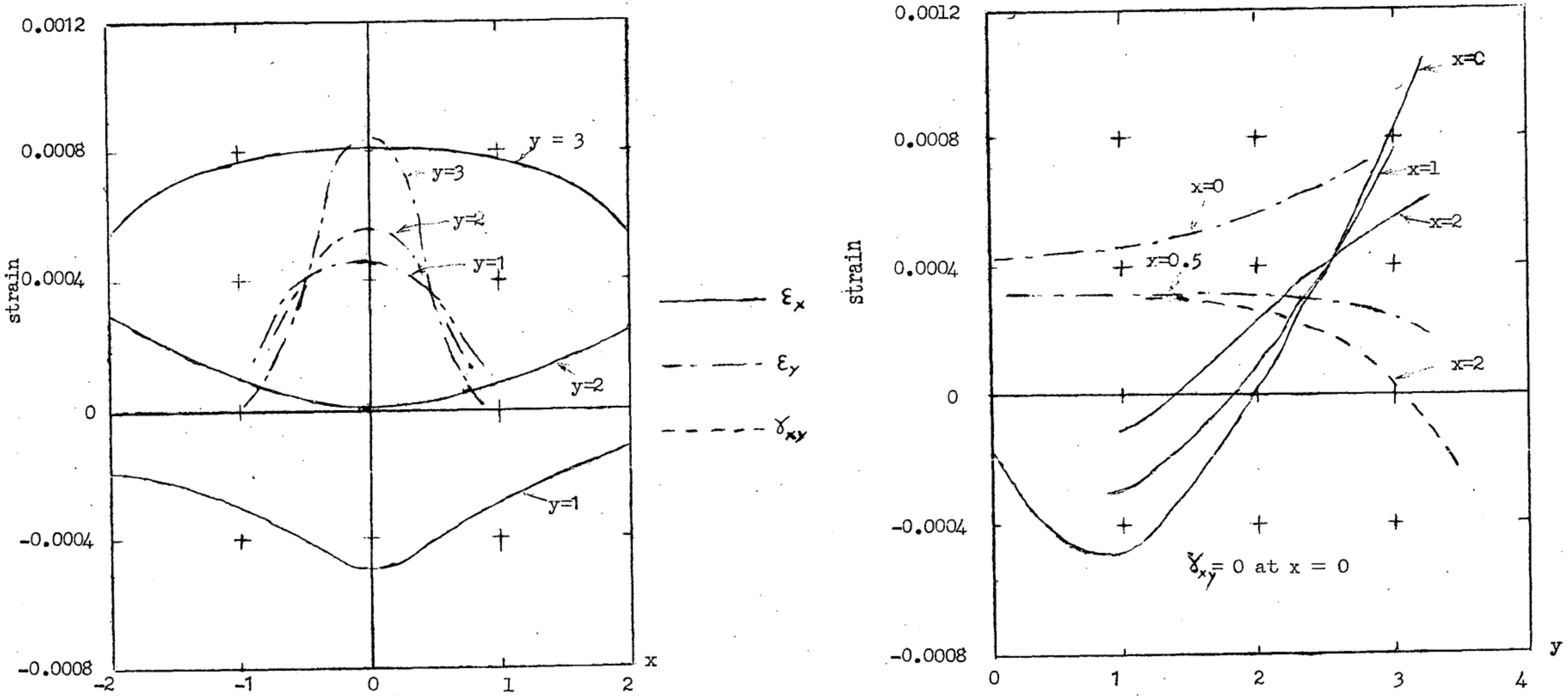

Fig. 27. S trains in Web of I-Section Knee.

4.3 Analytical Treatment of the Knee Problem

4.3.1 Energy Methods

Since the moire fringes show the functional form of the deformed shape of the model there is a strong temptation to use a strain energy method of analysis. If two guessed functions representing the u and v displacement curves and containing a number of free parameters are fed into a strain energy integral, the equation so constructed should provide a means of solving for the free parameters. The energy integral merely replaces some equations of statics which could have been solved directly, but the advantage of the energy method is that it provides a systematic means of choosing the equations of statics required (76). This method is essentially the same as that of Rayleigh.

Having obtained an approximate solution for the stress distribution by the above means, it should be possible to improve the solution by making a guess of statics based on the observed deficiencies of this first stress distribution, and using the complementary energy integral to take care of the equations of geometry in solving for the required parameters. This technique can of course be repeated indefinitely.

To illustrate the above procedure, consider a rectangular section beam in pure bending as shown in fig. 28.

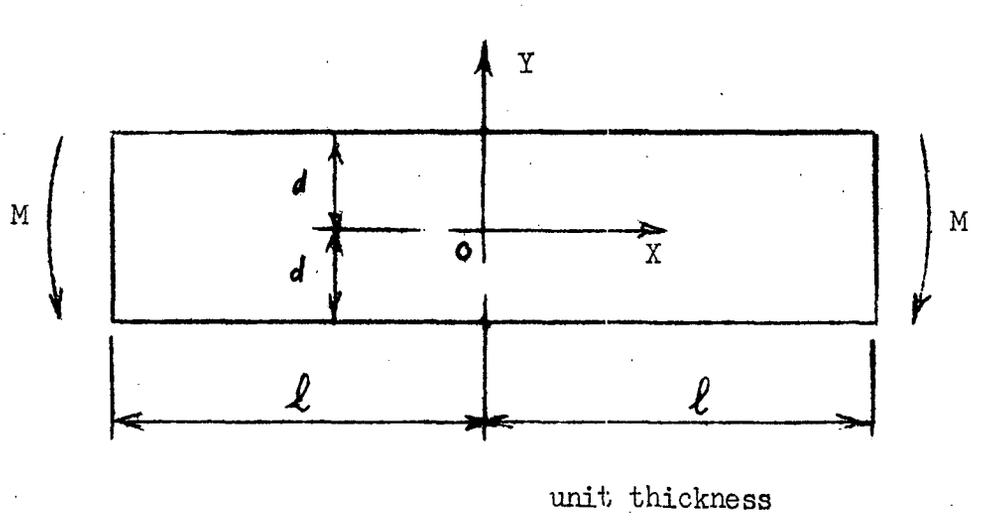

Fig. 28. Beam under action of Pure Bending.

A first estimate of geometry based on moire photographs of a beam of this type is

$$\left.\begin{aligned} u &= a_1 xy \\ v &= b_1 x^2 \end{aligned}\right\} \quad (xx)$$

where a_1 and b_1 are the free parameters whose values are to be determined. Strains and stresses are then given by

$$\varepsilon_x = a_1 y \qquad \sigma_x = H\, a_1 y$$

$$\varepsilon_y = 0 \qquad \sigma_y = H\, a_1 y$$

$$\gamma_{xy} = (a_1 + 2b_1)x \qquad \tau_{xy} = G(a_1 + 2b_1)x.$$

where $H = E/(1-\mu^2)$

E = Young's modulus

μ = Poisson's ratio

G = modulus of rigidity $= E/2(1+\mu)$.

The strain energy integral is usually written as

$$U = \int_{-\ell}^{\ell}\int_{0}^{\kappa} M\, d\kappa\, dx - \int_{-\ell}^{\ell}\int_{-d}^{d}\int_{0}^{\varepsilon_x} \sigma_x t\, d\varepsilon_x\, dxdy - \int_{-\ell}^{\ell}\int_{-d}^{d}\int_{0}^{y} \sigma_y t\, d\varepsilon_y\, dxdy$$

$$- \int_{-\ell}^{\ell}\int_{-d}^{d}\int_{0}^{\gamma_{xy}} \tau_{xy}\, t\, d\gamma_{xy}\, dxdy \qquad (xxi)$$

where U = strain energy

M = the moment at point x

κ = the path of M.

t = thickness (= 1 in this case.)

For structural analysis involving line segments, κ is the curvature of the segment and for small deformations

$$\kappa = \frac{\partial^2 v}{\partial x^2} \qquad (xxii)$$

and it would seem logical to write

$$\kappa = \left|\frac{\partial^2 v}{\partial x^2}\right| y = 0 \qquad (xxiii)$$

thus defining κ as the curvature of the neutral axis. However this expression is correct only when plane cross sections normal to the line of centroids remain plane, and it appears that rather more complex expressions have to be used in more general cases, a fact that has not been pointed out before to the writer's knowledge.

In the present case plane sections do remain plane ($\varepsilon_x = a_1 y$) and thus

$$\kappa = b_1$$

Differentiating the strain energy integral with respect to the free parameters a_1 and b_1 we have

$$\left.\begin{aligned} \frac{\partial U}{\partial a_1} &= 2M\ell - 4Ha_1\ell d^3/3 - 4Ga_1\ell^3 d/3 - 8G\, b_1\ell^3 d/3 = 0 \\ \frac{\partial U}{\partial b_1} &= G(8a_1\ell^3 d/3 + 16b_1\ell^3 d/3) = 0 \end{aligned}\right\} \text{(xxiv)}$$

Solving these equations we have

$$a_1 = 3M/2Hd^3 \; ; \quad b_1 = -3M/4Hd^3.$$

whence

$$\sigma_x = 3My/2d^3 \; ; \; \sigma_y = 3\mu My/2d^3 \; ; \; \tau_{xy} = 0 \qquad \text{(xxv)}$$

The expressions for σ_x and τ_{xy} in equation (xxv) satisfy the boundary conditions of statics, but the expression for σ_y does not. The simplest means of satisfying the boundary conditions is to put $\sigma_y = 0$. Hence a first estimate of statics is

$$\sigma_x = a_1 y \quad ; \; \sigma_y = 0 \qquad \text{(xxvi)}$$

and in order to satisfy the equilibrium condition

$$\left.\begin{aligned} \frac{\partial \sigma_x}{\partial x} + \frac{\partial \tau_{xy}}{\partial y} &= 0 \\ \frac{\partial \sigma_y}{\partial y} + \frac{\partial \tau_{xy}}{\partial x} &= 0 \end{aligned}\right\} \text{(xxvii)}$$

we must have

$$\tau_{xy} = 0 \qquad \text{(xxvi)}$$

hence

$$\varepsilon_x = a_1 y/E, \quad \varepsilon_y = \mu a_1 y/E \ , \quad \gamma_{xy} = 0$$

The complementary energy integral is

$$C = \int_{-\ell}^{\ell}\int_{0}^{M} \kappa \, dM dx - \int_{-\ell}^{\ell}\int_{d}^{d}\int_{0}^{\sigma_x} \varepsilon_x \, d\sigma_x \, dxdy \qquad \text{(xxviii)}$$

differentiating with respect to a_1,

$$\frac{\partial C}{\partial a_1} = \int_{-\ell}^{\ell} \frac{\partial M}{\partial a_1} \, dx + \frac{1}{E} \int_{-\ell}^{\ell}\int_{-d}^{d} a_1 y . y \, dxdy = 0$$

but

$$M = \int_{-d}^{d} \sigma_x \, y \, dy$$

$$= 2 a_1 d^3/3$$

therefore

$$2\kappa d^3 \ell/3 = 2a_1 d^3 \ell/3E.$$

$$a_1 = E\kappa.$$

Hence $\varepsilon_x = \kappa y \ ; \ \varepsilon_y = \mu \kappa y \ ; \ \gamma_{xy} = 0$ (xxix)

The last result satisfies the geometric boundary conditions and hence the solution

$$\sigma_x = 3My/2d^3 \ ; \ \sigma_y = \tau_{xy} = 0 \qquad \text{(xxx)}$$

is the exact solution to the problem.

The method illustrated above would be a simple and straightforward method of obtaining good approximations to the stresses and strains in a structure, were it not for the difficulties associated with the determination of the path followed by the moment (and by the shear and axial forces in more complex problems). The determination of latter quantities proved too awkward for the method to be useful, and therefore an alternative method of attack was adopted.

4.3.2 A Direct Method of Analysis

The method of analysis finally proposed consists of finding approximate expressions for the u and v displacement curves and using the conditions of statical equilibrium to solve for the free parameters in these expressions. However before describing this method a similar technique for finding the maximum stress in a straight, symmetrical knee joint will be presented. This technique was suggested by the author in previous work (75).

The maximum stress in a straight, rectangular section knee joint occurs at the internal corner of the joint. For a symmetrical knee the distribution of σ_x across the line x = 0 is represented, to a first approximation, by the equation

$$\sigma_x = a_1 y^2 + a_2 y \qquad \text{(xxxi)}$$

Values for the parameters a_1 and a_2 may be obtained using the relationships

$$P = \int_0^{d'} t\,(a_1 y^2 + a_2 y)\,dy$$

$$M_o = \int_0^{d'} t\,(a_1 y^2 + a_2 y)\,y\,dy \qquad \text{(xxxii)}$$

where P = normal force

M_o = moment about line y = 0

d' = width of knee measured along line y = 0

(see fig.29 , p. 74).

Table I shows the values of a_1 and a_2 and also of σ_x at $y = d'$, (the maximum stress in the knee) for the three rectangular section knees tested by the author. Also shown in this table are the corresponding experimental values for σ_x, and the percentage difference between the analytical and experimental solutions is shown.

TABLE I

	araldite Knee ‡	Small Perspex Knee	Large Perspex Knee
Load (lbs.)	54.9	57.7	51.5
t (ins.)	0.289	0.251	0.258
d' (ins)	1.600	1.623	3.248
a_1	2390	2550	244
a_2	-2400	-2570	-492
σ_x(anal)(psi)	2270	2550	981
σ_x(expt)(psi)	2190	2340	934
difference, %	3.8	9	5

‡ ref. (75).

(The stress values shown for the perspex knees are based on values of E and μ from bending and tension tests using Huggenberger tensometers. However these quantities show large variations even between pieces of the same sheet and variations of up to 15% between the values in orthogonal directions have been frequently reported. For this reason the experimental values for stresses are not reliable. However displacements have been checked by measuring the relative displacement between two points by means of Huggenberger tensometers, and the values obtained by this means have been within 3% of the values obtained from the moire photographs).

At other points across the section $x = 0$ the analytical solution provides values for σ_x with a similar accuracy to that at the internal corner. Since this section is a line of symmetry it is also a principal plane, i.e. $\tau_{xy} = 0$ and σ_x is also the maximum principal stress.

Application of this method to knees of variable cross-section is also possible. In the case of the I-section knee tested we find $a_1 = 186$, $a_2 = -510$ whence $\sigma_x = 770$ psi at $y = 3.828"$ (the internal corner). The corresponding experimental result is 879 psi, which is 12½% higher than

the analytical result. Part of this difference is due to shear lag in the flanges, which reduces the load carried by these members in the vicinity of the joint.

The experimental result for the stress given in the above paragraph is once again open to some doubt because of the variation in the values of E and μ, but a further possible source of error in this case was the glue joint. These joints were approximately 0.025" thick, and the unavailibility of Perspex glue of the type required led to the use of inferior quality glue and thus the interaction between web and flange may not have been as great as it would normally be.

The method described above provides estimates of the stresses across the line of symmetry ($x = 0$), but does not allow calculation of stresses (or strains) elsewhere. This is not, of course, always necessary, but where an estimate of these quantities is desirable the method to be described provides a next approximation. This analysis is based on approximate expressions for the u and v curves containing several free parameters, and using the conditions of statical equilibrium to find values for these parameters.

Choice of suitable expressions for the u and v patterns may not always be easy. The patterns for the rectangular section knee, for example, show superficial resemblance to the patterns for a simple beam, and yet an analysis based on simple beam theory is inadequate for the present purpose. However the graphs of strain, figs. 25,-27 (i.e. graphs of $\frac{\partial u}{\partial x}$ etc.)provide much help in this regard.

In the case of rectangular section knees a first approximation to the u and v curves is

$$\left.\begin{aligned} u &= a_1x^2 + a_2xy^3 + a_3xy^2 + a_4xy \\ v &= b_1x^2 \end{aligned}\right\} \quad \text{(xxxiii)}$$

in the region bounded by the lines

$$x = 0; \quad x = d' \; ; \quad y = mx \; ; \quad y = mx + d'$$

where m = slope of the edges of the knee with respect to the x - axis (see fig. 29).

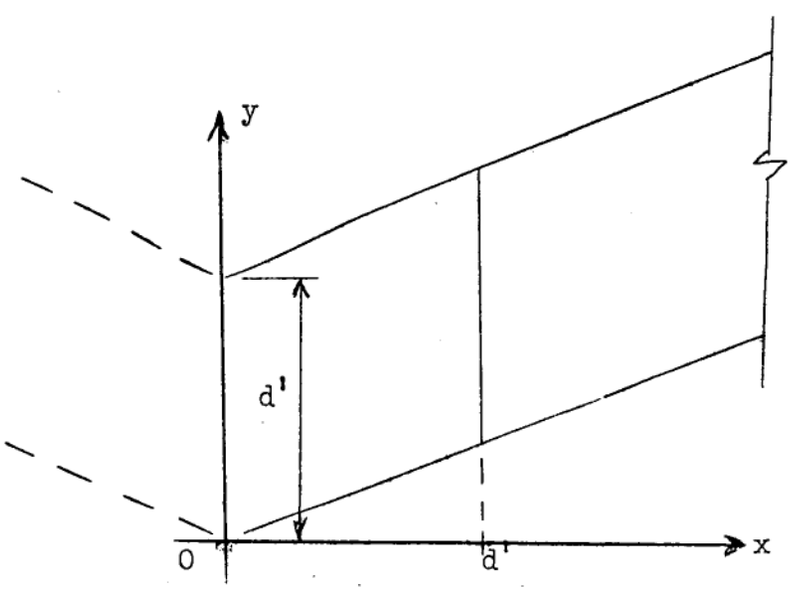

Figure 29, Knee Joint

Outside this region (i.e. between the lines $x = 0, d', y = mx, mx + d'$) normal engineering beam-column analysis may be used.

In the region under consideration, eq. (xxxiii) gives

$$\sigma_x = H(2a_1 x + a_2 y^3 + a_3 y^2 + a_4 y^1)$$

$$\sigma_y = H(2a_1 x + a_2 y^3 + a_3 y^2 + a_4 y)$$

$$\tau_{xy} = G(3a_2 xy^2 + 2a_3 xy + a_4 x + 2b_1 x) \; .$$

The equations of statics used here are

$$\int_{mx}^{mx+d'} \sigma_x \, t \, dy = P \quad ; \quad \int_{mx}^{mx+d'} \sigma_x \, y \, t \, dy = M_o \qquad \text{(xxxiv)}$$

$$\int_{mx}^{mx+d'} \tau_{xy} \, t \, dy = 0$$

For the small scale perspex knee (fig. 19) these equations may be satisfied along the boundaries $x = 0$, $x = d'$ by putting

$$a_1 = -0.000495 \quad ; \quad a_2 = -0.00479$$

$$a_3 = 0.0153 \quad : \quad a_4 = -0.00960$$

$$b_1 = -0.00113 \ .$$

(using E = 432,000 psi, $\mu = 0.35$, P = 57.7 lbs.)

Fig. 30 shows a comparison between this analytical result and the experimental results for ε_x across two sections of the knee. The analytical expression is not a good fit, but does provide an approximation to the experimental result. The agreement between analytical and experimental results is worse for the large scale knee (fig. 21) and so improvements will have to be made before the functions can be used as a design tool. However the method is capable of indefinite improvements, depending upon the desired accuracy. No further work has yet been carried out to find better functions for u and v, or to fit functions to the I-section knee, but the graphs and photographs provided in this thesis should allow a design method to be produced along similar lines.

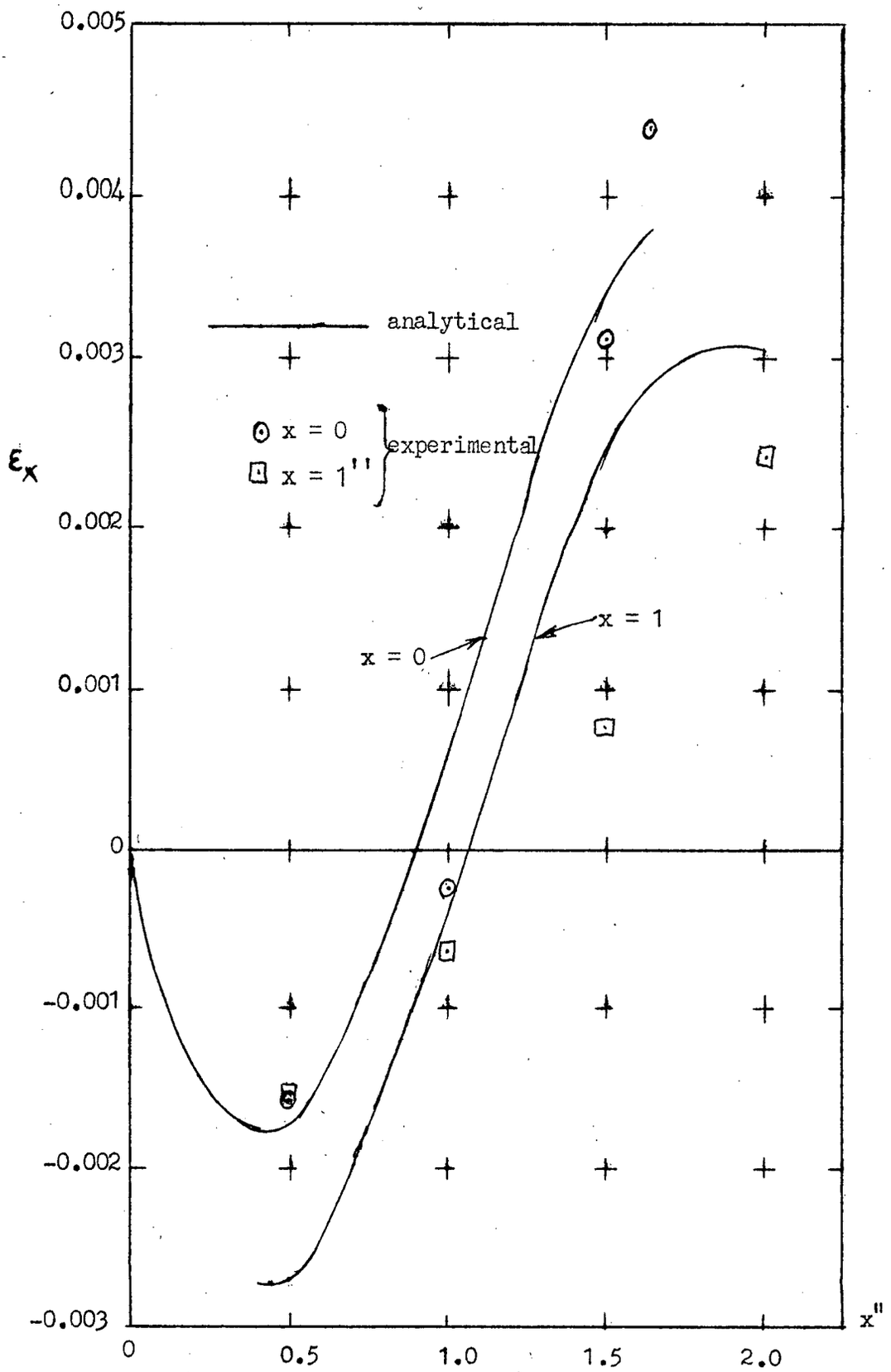

Fig. 30. Comparison of Analytical and Experimental Results for Small Scale Knee.

CONCLUSIONS

1. The techniques of making and using cheap diffraction gratings for a sensitive moire fringe method of strain analysis have been developed. The gratings have been used in transmission-type apparatus using transparent models. There appears to be little problem in using these in reflection once the problems of producing a reflecting surface and attaching the gratings have been overcome.

2. Gratings of 1000 and 3000 lines/in produced by these techniques were used to study some simple knee joints.

3. Some preliminary suggestions were made regarding the use of moire fringe patterns to develop analytical treatments suitable for use as a design tool.

4. A method for finding the maximum stress in a knee with moderate accuracy has been described. The method has been checked on all the knees tested, but applicability to knees with mitre angle other than 45° has not been investigated.

REFERENCES

1. GREGORY, M.S. Philosophy of Engineering Design of Structures. Journal of the Structural Division, A.S.C.E. Vol. 89, No. ST6, Proc. Paper 3722, December 1963 pp. 119-136

2. OLIVER, A.R. University Training of an Engineer. Institution of Engineers Australia, Tasmania Division Bulletin, no. 156, July 1965 pp 5-20

3. BREWER, G.A. Measurement of Strain in the Plastic Range. Proc. S.E.S.A., Vol I, no 2, 1943 pp 105-115.

4. DUNCAN, J.P. and BROWN, C.J.E. Slope Contours in Flexed Elastic Plates by Salet-Ikeda Technique. Proc. of First International Congress on Experimental Mechanics, Edited by B.E. Rossi, Pergamon Press; New York 1963. pp 149-176.

5. GUILD, J. The Interference Systems of Crossed Diffraction Gratings. Monographs on the Physics and Chemistry of Materials, Clarendon Press, Oxford, 1956.

6. GUILD, J. Diffraction Gratings as Measuring Scales. Oxford University Press, 1960.

7. MERTON, T. On the Reproduction and Ruling of Diffraction Gratings. Proc. Roy. Soc. London, Vol 201, series A, 1950. pp187-191.

8. DEW, G.D. and SAYCE, L.A. On the Production of Diffraction Gratings I: The Copying of Plane Gratings. Proc. Roy. Soc. London. Vol 207, series A, 1951. pp278-284

9. HALL, R.G.N. and SAYCE, L.A. On the Production of Diffraction Gratings II: The Generation of Helical Rulings and the Preparation of Plane Gratings Therefrom. Proc. Roy. Soc. London, Vol 215, series A, 1952 pp 536-550.

10. LORD RALEIGH (STRUTT, J.W.) On the Manufacture and Theory of Diffraction Gratings. Scientific Papers Vol. I Cambridge University Press, 1899. p 209. also Phil.Mag. Vol 47, 81-93, 193-205, 1874

11. BOUWKAMP, J.G. The Moire Method and the Evaluation of Principal Moment and Stress Directions. Experimental Mechanics, Vol, 4, no. 5, May 1964. pp 121-128.

12. COOKE, D. Moire Fringe Technique for Vibration Measurement. J. Sci. Instrum. , Vol 39, no. 7 July 1962. pp 373-376

13. CRISP, J.D.C. Measurement of Plane Strains by a Photoscreen Method. Proc. S.E.S.A. Vol XV, no 1. pp 65-76.

14. DANTU, P. Recherches Diverses d'Extensometrie at de Détermination Des Contraintes. Analyse des Contrantes, Mem du GAMAC. Vol. 2, no 2, Feb 1954. pp 3-22.

15. DANTU, P. Utilisation de Réseaux pour l'Etude Expérimental des Phénomènes Élastiques et Plastiques. Comptes Rendus Academie des Sciences, Paris. Vol 239, Dec 1954 pp 1769- 1771.

16. DANTU, P. Utilisation des Réseaux pour l'Etude des Déformations. Annales de l'Institut Technique du Batiment et des Travaux Publiques. no 121, Jan 1958. pp 78-98.

17. DANTU, P. Extension of the Moire Method to Thermal Problems. Experimental Mechanics, Vol 4, no 3. March 1964. pp 64-9

18. DANTU, P. Utilisation de la Méthode du Moiré pour l'Étude des Problèmesd'Élasticité à Trois Dimessions. Comptes Rendu, Academie des Sciences, Paris Vol 258, no 17. April 1964. pp 4206-7

19. DURELLI, A.J. and DANIEL, I.M. Structural Model Analysis by means of Moire Fringes. Journal of the Structural Division, A.S.C.E. Vol 86, no ST12, Proc. Paper 2693. December 1960 pp 93-102.

20. FRAPPIER, E. I Methodé Sensitométrique pour la Determination des Reseaux d'Isoclines.
II Etude d'une Interferomètr pour la Determination des Lignes Isopachiques. Analyse des Contraintes, Mem. du GAMAC. Vol 2, no 8, April 1957. pp 29-36.

21. LIGTENBERG, F.K. The Moire Method - A New Experimental Method for the Determination of Moments in Small Slab Models. Proc. SESA. Vol XII No 2, 1954. pp 83-98.

22. LOW, I.A.B. and BRAY J.W. Strain Analysis Using Moire Fringes. The Engineer, Vol 213, no 5540 March 1962 pp. 566-569.

23. MESMER, G. The Interference Screen Method for Isopachic Patterns (Moire Method). Proc. SESA, Vol XIII no 2, 1956. pp 21-26.

24. POST, D. A New Photoelastic Interferometer, Suitable for Static and Dynamic Measurements. Proc. SESA. Vol XII, no. 1. 1954 pp 191-202.

25. POST, D. Photoelastic Evaluation of Individual Principal Stresses by Large Field Absolute Retardation Measurements, Proc. SESA vol XIII, no 2, 1955 pp 119-132.

26. RILEY, W.F. and DURELLI, A.J. Application of Moire Methods to the Determination of Transient Stress and Strain Distributions, Journal of Applied Mechanics, Trans. ASME. Vol 29, Series E, No. 1 March 1962 pp 23-29.

27. SCIAMMARELLA, C.A. and ROSS, B.E. Thermal Stresses in Cylinders by the Moire Method. Experimental Mechanics, Vol 4, no 10 October 1964 pp 289-296.

28. SCIAMMARELLA, C.A. and CHIANG, Fu-pen. The Moire Method Applied to Three-dimensional Elastic Problems. Experimental Mechanics. Vol 4 no 11 November 1964 pp 313-319

29. SHEPHERD, R. and WENSLEY L.McD. The Moire-fringe Method of Displacement Measurements Applied to Indirect Structural - model Analysis. Experimental Mechanics, vol 5, no 6, June 1965 pp 167-176.

30. TANAKA, K.and NAKOSHIMA, M. Application of the Photograting Technique to the Measurement of Strain Produced at High Temperatures. Proc. the Japanese Congress on Testing Materials, Kyoto, 1963 pp 79-81

31. THEOCARIS, P.S. Isopachic Patterns by the Moire Method. Experimental Mechanics, Vol 4, no. 6 June 1964 pp. 153-159.

32. THEOCARIS, P.S. The Moire Method in Thermal Fields. Experimental Mechanics, Vol 4. no 8, August 1964 pp. 223-231.

33. THEOCARIS, P.S. and KUO, H.H. The Moire Method of Zonal and Line Gratings. Experimental Mechanics, vol 5, no 8, August 1965 pp 267-

34. THIRY, R. and DANTU, P. Expose General d'une Methode Experimental de Determination Directe des Deformations dans une Solide. 9th International Congress for Applied Mechanics, Bruxelles, 1957 pp 490-499.

35. VINKIER, A. and DECHAENE, R. Use of the Moire Effect to Measure Plastic Strains. Journal of Basic Engineering, Trans. ASME Vol 82, series D, 1960 pp.426-434

36. VREEDENBURGH, C.G.J. and WYNGAARDEN, H. New Progress in our Knowledge about the Moment Distribution in Flat Slabs by means of the Moire Method. Proc. SESA. Vol XII, no 2. 1954 pp 99-114.

37. THEOCARIS, P.S. Moire Fringes: A Powerful Measuring Device. Applied Mechanics Reviews, Vol 15, no 5, May 1962 pp 333-339.

38. SCIAMMARELLA, C.A. and DURELLI, A.J. Moire Fringes as a Means of Analysing Strains. Journal of the Engineering Mechanics Division, ASCE Vol 87 no EM1, Proc. paper no. 2736. Feb. 1961 pp 55-74.

39. TOLLENAAR, D. Moire-interferentieverschijnselen bij rasterdruk. Amsterdam Intitut voor Grahische Technick 1945.

40. WELLER, R. and SHEPARD, B.M. Displacement Measurement by Mechanical Interfermoetry. Society for Experimental Stress Analysis, Vol VI no. 1, 1948 pp 35-38.

41. KACZER, J. and KROUPA, F. The Determination of Strains by Mechanical Interference. Czechoslov.J.Phys., Vol I, 1952 pp 80-85.

42. DANTU, P. Correction à Apporter au Principe de l'Interpretation du Moiré quand les Déformations sont très Importantes. Laboratorie Central des Ponts et Chaussees, Paris. Internal Circ. Jan 21 1960 (A.M.R., Vol 15, no 5, p.336).

43. MORSE, S., DURELLI, A.J. and SCIAMMARELLA, C.A. Geometry of Moire Fringes in Strain. Analysis. Journal of the Engineering Mechanics Division, A.S.C.E. Vol. 86 no EM4, Proc. Paper no. 2576. August, 1960 pp.105-126.

44. DURELLI, A.J., SCIAMMARELLA, C.A. and PARKS, V.J. Interpretation of Moire Patterns. Journal of the Engineering Mechanics Division, A.S.C.E. Vol 89, No EM2, Proc. paper 3485, April 1963 pp 71-88.

45. TIMOSHENKO, S. and GOODIER, J.N. Theory of Elasticity. McGraw-Hill Book Company Inc., 1951

46. PIRARD, A. La Methode du Moiré en Photoelasticité. Revue Universelle des Mines, Vol 16, no 4, April 1960, pp 177-200.

47. OSTER, G., WASSERMAN, M. and ZWERLING, C. Theoretical Interpretation of Moire Patterns. Journal of the Optical Society of America, Vol 54, No 2. Feb 1964, pp 169-175.

48. CHIANG, Fu-pen. A Method to Increase the Accuracy of Moire Method. Journal of the Engineering Mechanics Division, ASCE. Vol 91, no EM1, Proc Paper no 4239, Feb 1965 pp 137-149.

49. DURELLI, A.J. and SCIAMMARELLA, C.A. Elastoplastic Stress and Strain Distribution in a Finite Plate with a Circular Hole Subjected to Unidimensional Load. Journal of Applied Mechanics, Trans ASME, Vol 30, series E, No 1. March 1963 pp 45-121

50. COKER, E.G. and FILON, L.N.G. A Treatise on Photoelasticity. Second Edition Revised by H.T. Jessop. Cambridge University Press 1957.

51. FROCHT, M.M. Photoelasticity John Wiley Vol I. 1941, Vol II 1948.

52. SCIAMMARELLA, C.A. Basic Optical Law in the Interpretation of Moire Patterns Applied to the Analysis of Strains. Part 1. Experimental Mechanics, Vol 5 no 5 May 1965. pp 154-160.

53. ROSS, B.E., SCIAMMARELLA, C.A. and STURGEON, P. Basic Optical Law in the Interpretation of Moire Patterns Applied to the Analysis of Strains. Part 2. Experimental Mechanics Vol 5, no 6. June 1965 pp 161-166.

54. DREW, G.D. On the Preservation of Groove Form in Replicas of Diffraction Gratings. Journal of Scientific Instruments, Vol 29, September 1952 pp 277-279.

55. DREW, G.D. On the Preparation of Plane Diffraction Grating Replicas from Helical Rulings. Journal of Scientific Instruments, Vol 30, July 1953 pp 229-232.

56. DREW, G.D. On preparing Plastic Copies of Diffraction Gratings An Extension to the Merton-N.P.L. Process. Journal of Scientific Instruments, Vol 33, no 9, September 1956 pp 348-353.

57. SAYCE, L.A. The Production of Diffraction Gratings. Endeavour, vol 12, no 48, 1953.

58. ———— Perspex Acrylic Materials; Cementing Imperial Chemical Industries Limited, Plastics Division

59. MIDDLETON, E. and JENKINS, C.J. A Moire Method of Strain Analysis for Student Use. Bulletin of Mechanical Engineering Education. (To be published).

60. GRAY, C.S. KENT, L.E., MITCHELL, W.A. and GODFREY, G.B. Steel Designers Manual. Second Edition. Crosby Lockwood, London 1960. pp 738-772

61. HENDRY, A.W. An Investigation of the Stress Distribution in Steel Portal Frame Knees. The Structural Engineer, March/April 1947. (Discussion December 1947).

62. HENDRY, A.W. An Investigation of the Strength of Welded Portal Frame Connections. The Structural Engineer, October 1950. (Discussion September 1951).

63. HENDRY, A.W. An Investigation of Certain Welded Portal Frames in Relation to the Plastic Method of Design. The Structural Engineer December 1950 (Discussion, Sept. 1951).

64. LYSE, I. and BLACK, W.E. An Investigation of Steel Rigid Frames. Trans A.S.C.E. Vol 107, Paper no. 2130, 1942. pp 127-186.

65. TOPRACTSOGLOU, A.A., BEEDLE, L.S. and JOHNSTON, B.G. Connections for Welded Continuous Portal Frames. Part I. The Welding Journal, Vol 30, no 7. July 1951 pp 359 s - 384 s.

66. BEEDLE, L.S., TOPRACTSOGLOU, A.A. and JOHNSTON, B.G. Connections for Welded Continuous Portal Frames Part II. Theoretical Analysis of Straight Knees. The Welding Journal, Vol 30, no 8, August 1951 pp 397 s- 405 s.

67. BEEDLE, L.S., TOPRACTSOGLOU, A.A. and JOHNSTON, B.G. Connections for Welded Continuous Portal Frames Part III Discussion of Test Results and Conclusions. The Welding Journal, vol 31, no 11, November 1952. pp 543 s - 560 s.

68. FISHER, J.W., DRISCOLL, G.C.(Jnr.) and SCHUTZ, F.W.(Jnr.) Behaviour of Welded Corner Connections. The Welding Journal, Vol 37, no 5, May 1958 p 216 s.

69. FISHER, J.W. and DRISCOLL, G.C.(Jnr.) Corner Connections Loaded in Tension. The Welding Journal, Vol 38, no.11, November 1959. pp 425 s - 434 s.

70. FISHER, J.W., LEE, G.C., YURA, J.A., and DRISCOLL, G.C.(Jnr.) Plastic Analysis and Tests of Haunched Corner Connections. Welding Research Council Bulletin, Eng. Foundation No 91, October 1963.

71. GROVER, L.M. Welded Structures: A Symposium Design and Research. Trans. A.S.C.E. Vol 120. Paper no .2729, 1955. pp. 112-146.

72. STANG, A., GREENSPAN, M., and OSGOOD, W.R. Strength of Rivetted Steel Rigid Frame Having Straight Flanges. Journal of Research, U.S. Nat. Bureau of Standards, Vol XXI, Research Report no 1130, 1938.

73. OLANDER, H.C. A Method for Calculating Stresses in Rigid Frame Corners. Proc. Struct. Division, A.S.C.E., Vol 79, Separate no 249, August 1953.

74. ———— Commentary on Plastic Design in Steel: Connections. Progress Report No. 6 of the Joint WRC-A.S.C.E. Cmtte. on Plasticity Related to Design. Journal of the Engineering Mechanics Division, ASCE Vol 86, No EM2, April 1960. pp 107-140.

75. JENKINS, C.J. Stresses in Rigid Frame Knees. Honours Degree Thesis, University of Tasmania, March 1964.

76. OLIVER, A.R. Energy Methods in Structural Analysis. Civil Engineering Transactions, Institution of Engineers, Australia, Vol CE.3, no 1, March 1961. pp 39-44.